Journal of Volcanology and Geothermal Research 297 (2015) 89–108

Contents lists available at ScienceDirect

Journal of Volcanology and Geothermal Research

journal homepage: www.elsevier.com/locate/jvolgeores

Volcano–ice–sea interaction in the Cerro Santa Marta area, northwest James Ross Island, Antarctic Peninsula

Fernando M. Calabozo [a,b,*], Jorge A. Strelin [a,c], Yuji Orihashi [d], Hirochika Sumino [e], Randall A. Keller [f]

[a] Centro de Investigaciones en Ciencias de la Tierra (CICTERRA-CONICET), Ciudad Universitaria, Córdoba X5016CGA, Argentina
[b] Universidad Nacional de Córdoba, Argentina
[c] Instituto Antártico Argentino (IAA)-Dirección Nacional del Antártico (DNA), Buenos Aires 1000-1499, Argentina
[d] Earthquake Research Institute, the University of Tokyo, Bunkyo, Tokyo 113-0032, Japan
[e] Geochemical Research Center, Graduate School of Science, the University of Tokyo, Bunkyo, Tokyo 113-0033, Japan
[f] Department of Geosciences, Oregon State University, Corvallis, OR 97331, USA

ARTICLE INFO

Article history:
Received 10 November 2014
Accepted 21 March 2015
Available online 28 March 2015

Keywords:
Subaqueous volcanism
Neogene
Glacial lithofacies
K–Ar dating
Glaciovolcanism

ABSTRACT

We present here the results of detailed mapping, lithofacies analysis and stratigraphy of the Neogene James Ross Island Volcanic Group (Antarctic Peninsula) in the Cerro Santa Marta area (northwest of James Ross Island), in order to give constraints on the evolution of a glaciated volcanic island. Our field results included recognition and interpretation of seventeen volcanic and glacial lithofacies, together with their vertical and lateral arrangements, supported by four new unspiked K–Ar ages. This allowed us to conclude that the construction of the volcanic pile in this area took place during two main eruptive stages (Eruptive Stages 1 and 2), separated from the Cretaceous bedrock and from each other by two major glacial unconformities (U1 and U2). The U1 unconformity is related to Antarctic Peninsula Ice sheet expansion during the late Miocene (before 6.2 Ma) and deposition of glacial lithofacies in a glaciomarine setting. Following this glacial advance, Eruptive Stage 1 (6.2–4.6 Ma) volcanism started with subaerial extrusion of lava flows from an unrecognized vent north of the study area, with eruptions later fed from vent/s centered at Cerro Santa Marta volcano, where cinder cone deposits and a volcanic conduit/lava lake are preserved. These lava flows fed an extensive (>7 km long) hyaloclastite delta system that was probably emplaced in a shallow marine environment. A second unconformity (U2) was related to expansion of a local ice cap, centered on James Ross Island, which truncated all the eruptive units of Eruptive Stage 1. Concomitant with glacier advance, renewed volcanic activity (Eruptive Stage 2) started after 4.6 Ma and volcanic products were fed again by Cerro Santa Marta vents. We infer that glaciovolcanic eruptions occurred under a moderately thin (~300 m) glacier, in good agreement with previous estimates of paleo-ice thickness for the James Ross Island area during the Pliocene.

1. Introduction

The reconstruction of eruptive environments within insular and glaciated volcanic terrains can be a difficult task, especially in old (pre-Quaternary) sequences. The James Ross Island Volcanic Group (JRIVG) is one of the largest Cenozoic mafic volcanic fields of Antarctica (Smellie, 1990) and represents an excellent example of such terrains, given that it records a long history (~6 Myr) of volcano–ice and volcano–sea interactions. JRIVG was formed by late Miocene-Recent alkali basaltic lavas which interacted in different degrees with external water (i.e., seawater and glacial ice) (Smellie, 1999; Smellie et al., 2006a, 2008). The presence of fossil-bearing marine and glacial strata, intimately associated with eruptive units, are important proxies to help unravel this region's paleoclimatic and volcanic history for the last ~6 Myr (Smellie et al., 2006a, 2008, 2009; Hambrey et al., 2008; Williams et al., 2010; Nývlt et al., 2011). Several publications, concerned with the eruptive history of JRIVG (see Smellie, 2006; Smellie et al., 2008), chose a rather regional approach, covering the bulk of the JRIVG. However, detailed studies over small areas are fundamental to construct a clearer picture of its volcanic evolution. This includes full understanding of their relationships with epiclastic strata, recognition of unconformities between different units and the discovery of undocumented eruptive centers.

James Ross Island is considered a large polygenetic shield volcano and Mt. Haddington (Fig. 1, 64.21°S–57.63°W) seems to be the main vent area (Smellie, 1990). However, in some areas of the James Ross Island (Ulu Peninsula, Fig. 1) volcanic strata dip towards the ice-capped Mt. Haddington volcano, implying that some of the eruptive units were emitted from satellite vents (see Smellie et al., 2008; Nehyba and Nývlt, 2014). One of these locations is the Cerro Santa Marta area,

* Corresponding author at: Centro de Investigaciones en Ciencias de la Tierra (CICTERRA), Argentina. Tel.: +54 351 5353800 int. 30237.
E-mail addresses: fcalabozo@efn.uncor.edu, fercalabozo_geo@yahoo.com.ar (F.M. Calabozo).

http://dx.doi.org/10.1016/j.jvolgeores.2015.03.011
0377-0273/

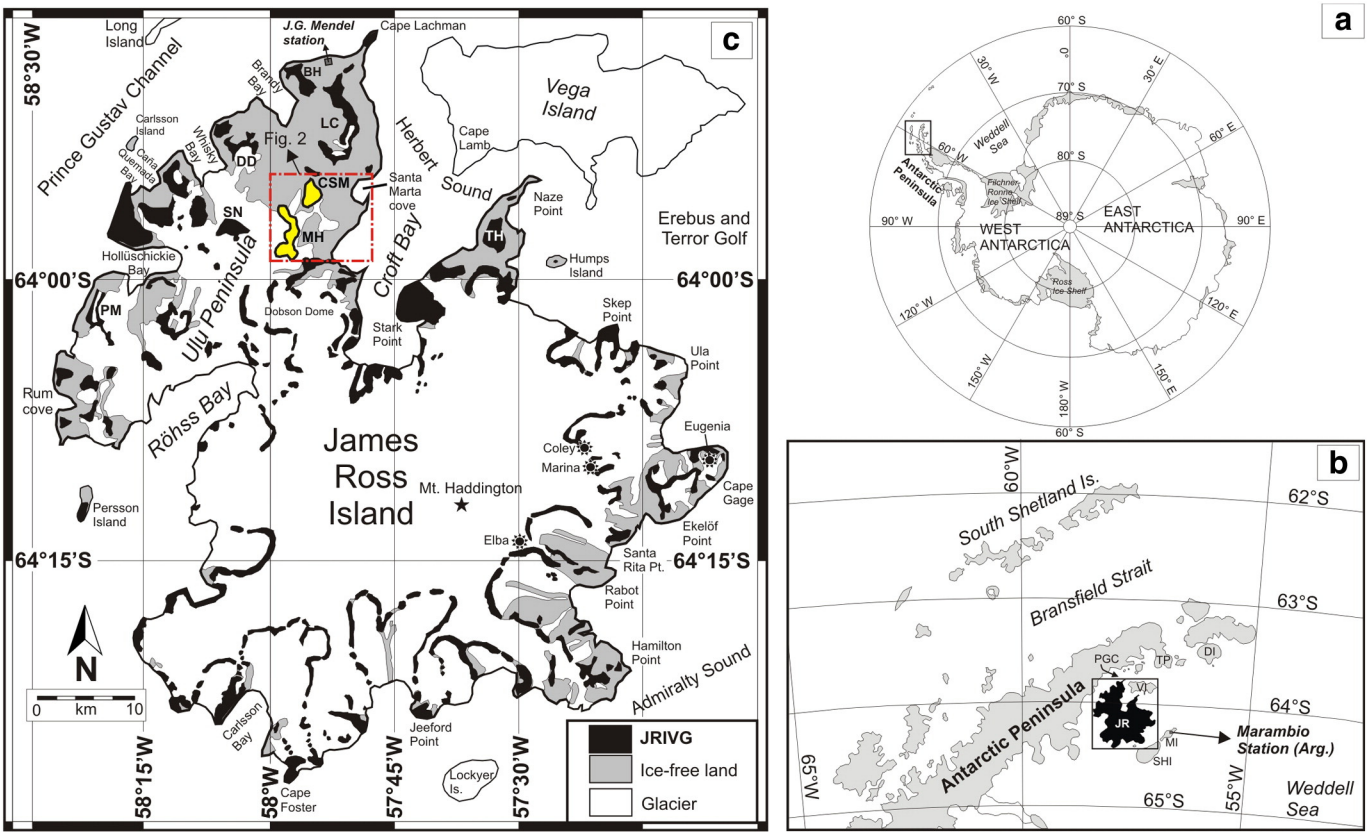

Fig. 1. Location map showing: a. the Antarctic continent with a box marking the northern tip of the Antarctic Peninsula, b. Antarctic Peninsula's northern tip, showing the location of James Ross Island (inset box) and the Argentine Marambio station, and c. James Ross Island map, showing the outcrops of the James Ross Island Volcanic Group (JRIVG), the ice-free and ice-covered terrain. The dashed red square marks the study area in Fig. 2. Cerro Santa Marta/Smellie Peak (CSM) and Massey Heights (MH) are highlighted in yellow. Eugenia, Coley, Marina and Elba refer to four Holocene monogenetic volcanoes. The J.G. Mendel station (Czech Republic) is also shown. Other localities discussed in the text are also shown. Key for abbreviations: JR James Ross Island, VI Vega Island, SHI Snow Hill Island, MI Marambio/Seymour Island, TP Tabarin Peninsula, DI Dundee Island, PGC Prince Gustav Channel, PM Patalamon Mesa, TH Terrapin Hill, LC Lachman Crags, DD Davies Dome, SN Seacatch Nunataks, BH Bibby Hill. (For interpretation of the references to color in this figure legend, the reader is referred to the web version of this article.)
Adapted from Strelin and Malagnino (1992).

in the northwest region of James Ross Island (Fig. 1). It includes two volcanic hills, Cerro Santa Marta and Massey Heights, where foreset beds dip towards Mt. Haddington. Therefore, an eruptive vent located northwest of Mt. Haddington is more probable, as originally noted by Strelin et al. (1987). We present here our stratigraphic interpretation of the volcano-epiclastic succession within the Cerro Santa Marta area, based on detailed field mapping, lithofacies description, and unspiked K–Ar dating, which allowed us to postulate that at least two main eruptive centers within this region acted as peripheral vents of the Mt. Haddington shield volcano, during late Miocene/early Pliocene times. These vents were most likely responsible for the deposition of the volcanic pile now exposed at Massey Heights. Our results provide new insights into James Ross Island's volcanic eruptive environments and their chronological evolution together with paleoclimatic implications for the area during late Miocene/early Pliocene times.

2. Geological background

2.1. Geographic location and geochronology of the JRIVG

The JRIVG comprises a suite of back-arc alkaline basalts (Hole et al., 1995; Košler et al., 2009) widely distributed over more than 5000 km^2 between 63.5° and 64.5°S on the eastern side of the Antarctic Peninsula (Fig. 1), and whose eruptions took place over a long period of time (>6 Myr). The most voluminous and best exposed outcrops are found on James Ross and Vega Islands (Fig. 1). James Ross Island, with an area exceeding 2500 km^2 and a N–S length of ~65 km, is the largest island on the east side of the Antarctic Peninsula, from which it is separated by a narrow (10–20 km) and deep (~1280 m) sea strait known as Prince Gustav Channel (Fig. 1). The northwestern region of the island, referred to as Ulu Peninsula (Fig. 1), is a less glaciated area characterized by tidewater outlet glaciers, different types of valley glaciers and minor ice caps on top of volcanic mesas (Strelin and Malagnino, 1992; Engel et al., 2012), which provides accessible and well-exposed eruptive units. Less voluminous basaltic outcrops are found on several smaller volcanic islands along Prince Gustav Channel, reaching as far north as Cape Purvis on Dundee Island (Fig. 1, Smellie et al., 2006b). Within the Antarctic Peninsula overall, JRIVG localities are restricted to Tabarin Peninsula (Skilling, 1994; Smellie et al., 2006b). To the east of James Ross Island, on Marambio/Seymour and Snow Hill Islands (Fig. 1), JRIVG is represented by basaltic dikes and plugs intruding Cretaceous–Paleogene sedimentary rocks (Massabie and Morelli, 1977). Overall, the maximum thickness of the JRIVG probably reaches more than 1400 m at Mt. Haddington (Smellie, 1990).

Earlier geochronological studies using the conventional K–Ar method (Rex, 1976; Massabie and Morelli, 1977; Sykes, 1988; Lawver et al., 1995), together with more recent $^{40}Ar/^{39}Ar$ dating (Kristjánsson et al., 2005; Smellie et al., 2006a, 2006b, 2008; Nývlt et al., 2011) showed that *in-situ* outcrops afford ages between ~6.2 Ma (late Miocene) and ~0.13 Ma (late Pleistocene), but eruptions probably started as far back as ~12 Ma (Marenssi et al., 2010). With the available geochronological and field data, Smellie et al. (2008) concluded that at least fifty eruptions built the volcanic pile in ~6 Myr. The presence of four pristine monogenetic cones (Eugenia, Coley, Marina and Elba in Fig. 1), erupted

over Mt. Haddington's ice cap, suggests that volcanic activity continued into the Holocene (Strelin et al., 1993). However, there are no available radiometric ages for these pyroclastic monogenetic volcanoes that we know of.

2.2. Eruptive environment/s of the JRIVG

The most prominent feature of JRIVG is voluminous (tens of km^3) sequences of stacked lava-fed deltas, which unconformably overlie tilted marine Cretaceous sediments part of the James Ross basin (del Valle et al., 1992). Lava-fed delta sequences are formed by subhorizontal lava flows capping foreset-bedded, palagonitized hyaloclastite breccias, dipping at high angles (~15–30°) (Jones and Nelson, 1970; Nelson, 1975). These features indicate the entrance of subaerial, mostly pāhoehoe-type lava flows, into a large body of water (Jones and Nelson, 1970), which leads to lava fragmentation and gravity-driven deposition of volcanic debris (mostly pillow fragments) downslope. Breccia sheets will start to prograde as clinoforms, leading to the formation of coarse-grained volcaniclastic deltas, similar to their sedimentary analogs, Gilbert-type alluvial deltas (Porębski and Gradzinski, 1990; Skilling, 2002). The zone where a subaerial, initially coherent lava flow will suffer fragmentation (explosive or non-explosive) due to direct contact with external water is commonly referred as passage zone and is classically considered a good indicator of paleo-level of the water body (e.g., Jones and Nelson, 1970; Smellie, 2006) at the moment of lava-fed delta emplacement, although some problems may arise with this interpretation, especially when considering passage zones as paleo-shoreline indicators (see Watton et al., 2013). However, as pointed out by these same authors, in settings where the pāhoehoe lava flux is high due to coalescence into larger inflated sheets (Self et al., 1998), the fragmentation front at the delta leading edge quickly develops and advances in the sense of delta progradation, which may translate in

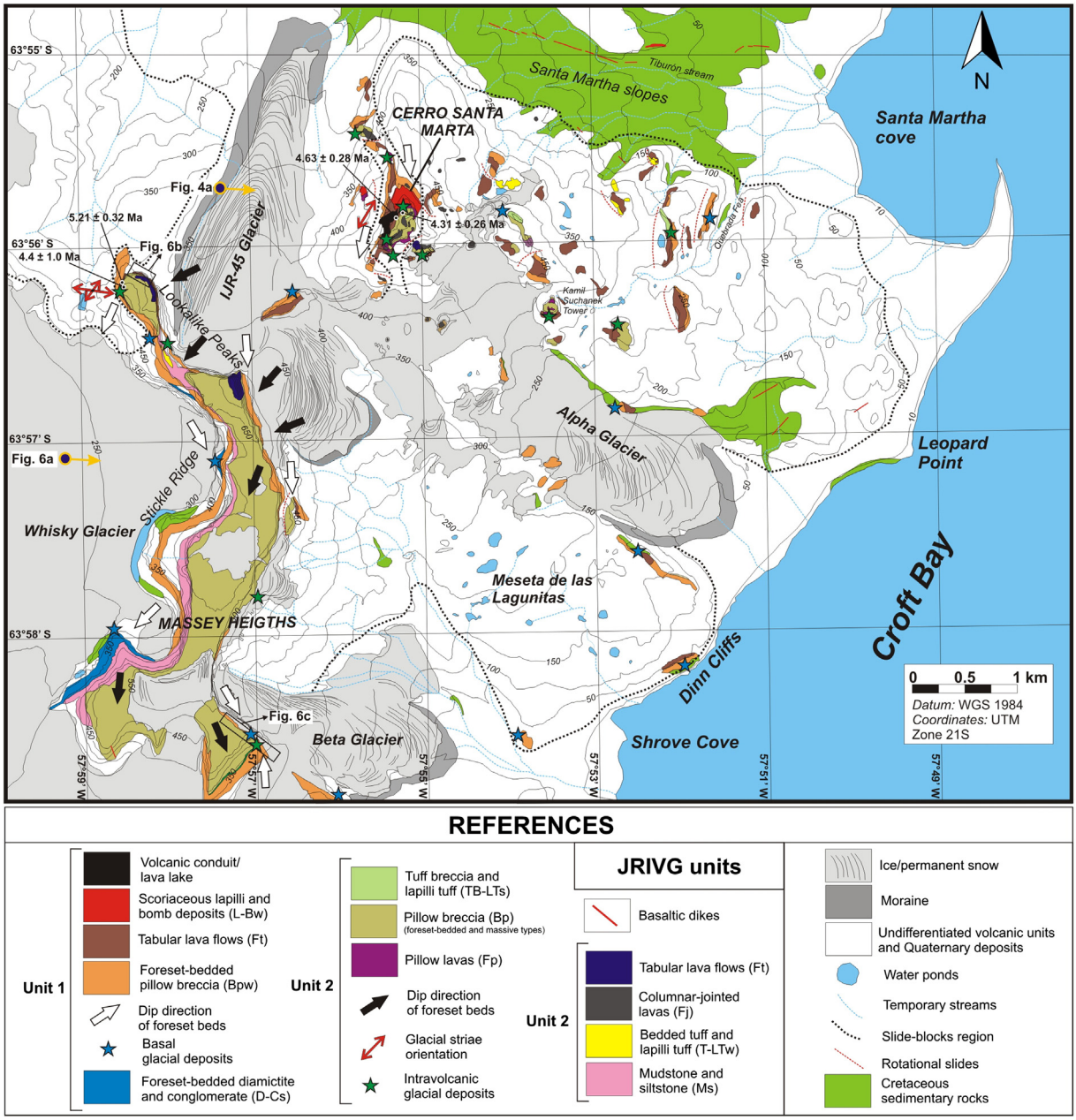

Fig. 2. Geological map of the Cerro Santa Marta area based on aerial photographs and our own field work. The contour lines are taken from the James Ross Island 1:25,000 topographic map (Czech Geological Survey, 2009) with an interval of 50 m, except for the 10 m line. Stars indicate the recognized but not mappable glacial diamictite outcrops. Locations of samples dated by K–Ar method are also shown.

well-defined passage zones, as is the case in the JRIVG (Skilling, 2002). Thus, in this case, passage zones are good proxies of paleo-water levels and the thickness of the subaqueous portion of the delta (i.e., foreset-bedded pillow breccias) may be considered a good approximation of the available accommodation space at the time of delta emplacement (i.e., water depth). Moreover, the geometries of well-defined passage zones (i.e., JRIVG) may help unravel the nature of the coeval water body at the time of lava-fed delta emplacement (Smellie, 2006).

For the JRIVG, Nelson (1975) inferred that lava-fed deltas were emplaced in a marine setting and concluded that variations in passage zone height represented eustatic sea level changes at the time of volcanic activity. Carrizo et al. (1998) agreed with Nelson's (1975) interpretation, but they postulated that passage zone height changes do not necessarily represent eustatic sea level oscillations. A different interpretation was given by several authors (Smellie et al., 1988; Smellie, 1990, 1999; Hambrey et al., 2008), who proposed that the bulk of the JRIVG was emplaced in a glaciovolcanic setting (i.e., volcanic products formed as some kind of lava–ice interaction; Smellie, 2006), given the close association between volcanic and glacial lithofacies. Moreover, abrupt changes in passage zone altitudes reflect a very dynamic water system with constant variations in the water level in a short time, which are difficult to explain by long-term eustatic sea level variations, but can be more typical of englacial settings (Skilling, 2002; Smellie, 2006; Smellie et al., 2008). Nevertheless, several tuff cone deposits of variable ages were probably emplaced in a marine setting, given the presence of marine fossils, such as the case of the late Miocene tuff cone deposits from Patalamon Mesa (Fig. 1), where asterozoans moulds are perfectly preserved at ~300 m above the present sea level (Williams et al., 2006). Terrapin Hill (Fig. 1) is another example of a marine-emplaced tuff cone during Pleistocene times (Smellie et al., 2006a). In some locations (Lachman Crags and Hamilton Point, Fig. 1), constant passage zone altitudes over several kilometers suggest a marine emplacement for those lava-fed deltas (Smellie et al., 2006a, 2008).

Associated with volcanic rocks, many mixed and pure glacial strata are found overlying the Cretaceous bedrock as well as interbedded within the volcanic succession. These glacial (both subglacial and glaciomarine) deposits, locally bearing marine shell remains, are important paleoclimatic proxies, and thus the focus of many detailed sedimentological and paleontological studies (Bibby, 1966; Pirrie et al., 1997; Strelin et al., 1997; Jonkers, 1998; Jonkers et al., 2002; Lirio et al., 2003; Hambrey and Smellie, 2006; Nelson et al., 2009; Williams et al., 2010; Nývlt et al., 2011) that showed that both glacial and interglacial conditions existed during Neogene times. Moreover, strontium isotope measurements on marine shells also give time constraints related to cyclicity of warmer, ice-poor conditions (interglacials) and cold, glacial periods (Smellie et al., 2006a; Nelson et al., 2009; Nývlt et al., 2011; Pirrie et al., 2011).

3. Methodology

We performed our field work during the austral summers of 2008, 2010, 2012 and 2014. The geological mapping was supported by satellite and aerial imagery, together with detailed field observations (Fig. 2). Stratigraphic logs were made at several locations but only the thirteen most representative logs are presented (Fig. 3). The logging methodology involved: bed thickness measurement using different

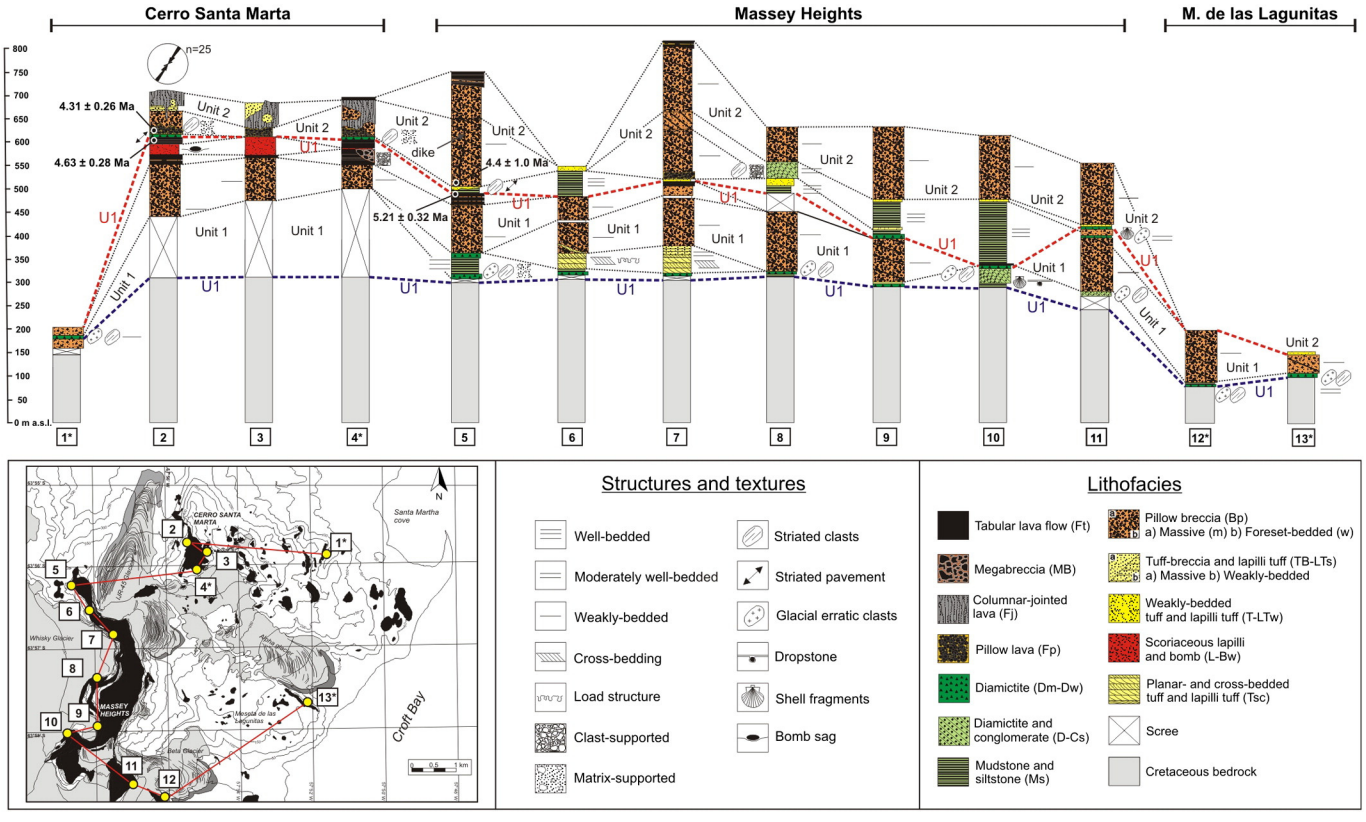

Fig. 3. Representative stratigraphic logs from Cerro Santa Marta and Massey Heights. Log locations are shown in the inset map. Logs 1 to 4 show the general stratigraphy at Cerro Santa Marta, whereas logs 5 to 13, including those from Meseta de las Lagunitas, represent the Massey Heights succession. The logging key for textures and sedimentary structures is adapted from Hambrey and Glasser (2003). Asterisks indicate stratigraphic logs constructed from slide-blocks. New unspiked K–Ar ages are shown on stratigraphic logs 2 and 5. Thick, dashed blue and red lines indicate unconformity U1 and U2, respectively. Rose diagram of clast fabric pattern of 25 clasts (n) from the glacial diamictite in log 2, found at 620 m a.s.l. Note the strong SW–NE clast orientation. For detailed log descriptions see the electronic Supplementary material. (For interpretation of the references to color in this figure legend, the reader is referred to the web version of this article.)

Table 1
Summary of volcaniclastic, coherent and glacial lithofacies, including a brief description and interpretation. For more detailed descriptions see the electronic Supplementary material. Key to abbreviations: CSM Cerro Santa Marta, MH Massey Heights, LM Meseta de las Lagunitas.

Lithofacies	Code	Thickness (m)	Locality	Description	Interpretation
Volcaniclastic lithofacies					
Foreset-bedded pillow breccia	Bpw	~200	CSM–MH	Pillow breccias, weakly cross-stratified, planar to tangentially, foreset-bedded and intensely palagonitized. Bed dips between 15 and 30°. Form sets 30–80 m thick. Internally, beds are matrix-supported, massive and rarely show evidence of grading, but when present is usually inverse. Bedding is diffuse and contacts between beds are sharp to gradational. Clasts are pillow-derived fragments (Fig. 7d). Matrix is composed of lapilli-sized vitroclasts, although more crystalline clasts are present. Vitroclast's shapes are variable, but equant and poorly-vesiculated clasts prevail, which shows sharp curvilinear or vesicle-bounded edges.	Hyaloclastite breccias formed by quenching and predominantly non-explosive fragmentation of subaerially-erupted lava flowing into a water body, forming a hyaloclastite delta front. Deposition from mass-wasting to avalanching.
Massive pillow breccia	Bpm	45	CSM–MH	Pillow breccias, massive to very poorly-bedded, laterally grading to massive pillow lavas (Fp). Also interbedded between subhorizontal tabular lava flows (Ft). Petrographic characteristics are similar to Bpw subtype, with predominance of equant and poorly-vesiculated clasts, with sharp curvilinear or vesicle-bounded edges.	Subaqueous, gravity-driven re-sedimentation of pillow lavas by gravitational mass-wasting. Layers between Ft lithofacies indicate that these lava flows entered a water body.
Tuff breccia and lapilli tuff	TB–LTs	35	CSM–MH	Matrix- to clast-supported, massive tuff breccia beds (30 to 45 cm thick) and alternation of thinner lapilli tuff beds (15–25 cm thick), with common lenticular geometries and bed amalgamation. Thicker beds usually show normal grading (Fig. 5f), but crude reverse grading is also common. Cross-bedding with large wave lengths is also observed. Basaltic clasts range from completely glassy pillow rims to holocrystalline massive basalt clasts. The matrix is composed fine lapilli and ash vitroclasts with blocky and equant shapes, and flat and curvilinear edges (Fig. 5g).	Fragmentation processes varied from non-explosive magma quenching (tuff breccia beds) to more explosive magma–water interaction (lapilli tuff beds). Deposition mechanism was concentrated, subaqueous cohesionless debris flows. The massive, clast-supported tuff breccias are probably related to sudden, gravitational mass-flow deposits.
Weakly-bedded tuff and lapilli tuff	T–LTw	25	MH–CSM–LM	Yellow coarse tuffs and lapilli tuffs, matrix- to clast-supported with medium to very thick planar-bedding (Fig. 7e). Common normal grading. The beds are composed mainly of glassy, variable vesiculated lapilli-sized juvenile vitroclasts, with very rare occurrence of accidental, crystalline, non-vesiculated basalt lithoclasts. The matrix is composed of highly-vesiculated ash-sized vitroclasts, with spherical to elongated vesicles. Vitroclasts edges are usually irregular, bounded by vesicle walls, but sharp and planar edges are also discernible, commonly in the vesicle-poor vitroclasts (Fig. 7f).	Tephra jets product of Surtseyan-type explosive hydromagmatic eruptions, in a shallow water body. Deposition as fallout and/or vertical density currents. The lack of evident lamination indicates high magma output, product of continuous tephra uprush.
Planar- and cross-bedded tuff and lapilli tuff	Tsc	15	MH	Thinly- to thickly-laminated yellow tuffs (beds between 10 and 60 cm thick) with minor proportion of lapilli tuffs and alternating beds with cross- and planar-bedding. Small scale cross-beds are formed by well-developed, B-type climbing ripples. Channel-like beds, with erosive basal contacts and lapilli-rich beds with normal grading are also observed.	Pyroclastic tuff material deposited in low flow regime conditions, product of tractional unidirectional flow.
Mudstone and siltstone	Ms	100	MH	Flat-lying, rhythmically-laminated, greenish mudstones and siltstones. Each bed is internally massive and between 1 and 15 cm thick. Lamination is planar. At several locations, contacts with T-LTw lithofacies are usually product of load deformation caused by the thick pile of pillow breccias overlying both lithofacies (see Fig. 6b). In thin section, this lithofacies is too fine-grained for component recognition but volcanic ash predominates.	Distal layer-by-layer deposition (delta bottomset) of fine tephra particles (subaqueous ash plume) product of high-density sediment gravity flows.
Scoriaceous lapilli and bomb	L–Bw	35	CSM	Reddish scoriaceous lapilli and bomb beds (Fig. 5d), medium to very thickly-bedded and matrix- to clast-supported. Poor welding predominates, although welded deposits (spatter) are locally abundant, formed by highly-flattened and coalesced scoriaceous bombs with lower percentage of lapilli matrix. In proximal sections, beds are commonly massive and include higher percentage of fluidal and spindle bombs (Fig. 5d), whereas in distal parts beds are lapilli-rich, clast-supported, and inversely graded.	Product of strombolian and hawaiian eruptive activity in a central vent (i.e., cinder cone).
Megabreccia	MB	40	CSM	Clast-supported megabreccia forming a wedge-shaped deposit. Consist in very poorly-sorted, monomict lithic breccias. Crystalline, mostly angular and subangular, oxidized, up to 2 m in diameter basalt clasts are the main constituents. Jigsaw-fit structures are very common, as well as prismatic joints and cooled edges. Matrix is extremely scarce and is constituted by non-vesiculated ash shards.	Volcanic debris avalanche product of "hot" deposition, probably during eruption. Collapse product of dike injection or flank collapse.

(continued on next page)

Table 1 (*continued*)

Lithofacies	Code	Thickness (m)	Locality	Description	Interpretation
Coherent lithofacies					
Tabular lava	Ft	50	CSM–MH–LM	Subhorizontal, stacked and tabular compound lava flows (Fig. 5c), with variable flow unit thickness between 0.5 and 4 m. Holocrystalline massive cores, with flow aligned vesicles, reddish scoriaceous bases and tops, where ropy textures are also common. Jointing is rare, but platy joints are observed.	Subaerial, inflated pāhoehoe-type lava flows.
Pillow lava	Fp	45	CSM–MH	Massive pillow lava lobes with mound-like morphology (Figs. 4 and 5d). Pillow lobe cross-sections are ellipsoidal, subspherical and slightly flattened, with massive to poor-vesiculated, porphyritic cores and glassy rims between 1 and 3 cm thick. The pillow lobes dip in different directions with angles of up to 15°. Inter-pillow space is usually filled with lenticular patches of palagonitized, non-vesicular glassy lapilli.	Subaqueous eruptions under high hydrostatic pressure, low effusion rates, gentle slopes and high cooling rates.
Columnar-jointed lava	Fj	70	CSM	Lavas with columnar-jointing of the entablature-type, fed by relatively thin subvertical dikes and characterized by small diameter columns (<30 cm) with irregular to chaotic column orientations (Fig. 4). A clast-supported, massive to weakly-bedded lithic breccia carapace, with palagonitized matrix, is in direct contact with this unit trough gradational contacts. The basalt clasts of this breccia are lithologically indistinguishable from the columnar-jointed lavas. Small (<2 cm) peridotite xenoliths are found.	Subaqueous intrusive/extrusive lava flow. Carapace breccia interpreted as in-situ mechanical rupture of basaltic bodies due to direct contact with external water.
Plugs, dikes and other intrusives	P	–	CSM–MH	The most important intrusive body found in the region is exposed at the west face of CSM. This dolerite intrusive has a gross lopolith-like morphology, with well-developed columnar-jointing in the lower sections (Figs. 4 and 5c). Dikes are commonly found intruding both the Cretaceous bedrock and the volcanic successions. At MH, ellipsoidal intrusives are found at the nearly horizontal contact between the Cretaceous substrate and the volcanic succession.	CSM intrusive body is interpreted as remnant of an eroded volcanic conduit or a lava lake. Dikes and other intrusives may have acted as secondary feeder systems.
Glacial lithofacies					
Weakly-bedded diamictite	Dw	13	CSM–MH–LM	Diamictite, clast-rich (~30% of clast content), with muddy to sandy matrix and boulder to cobble sized clasts. Weak bedding is marked by lenses of finer material and different accumulations of clasts. Clast lithologies include JRIVG-derived basalts, Cretaceous sedimentites and erratic (exotic) lithologies derived from the Antarctic Peninsula such as low-grade metamorphic rocks, granites and altered volcanic rocks (Fig. 5a). Clast facetting is common while striation is rare or absent. Also found are irregular, unconsolidated rip-up gravelly-sand lenses (Fig. 5b).	Flow till deposited close to the glacier melt-out zone near the grounding-line. The occurrence of gravelly-sand lenses is interpreted here as products of subglacial streams (glaciofluvial sediments) incorporated as rip-up clasts.
Massive diamictite	Dm	10	CSM–MH	Massive, matrix-supported diamictite, which grades from clast-poor (<10%) to clast-rich (>10%) varieties. Composed of floating clasts of up to 45 cm in diameter with a strong fabric orientation (SW–NE). The clasts are angular to subangular, in places showing bullet-shape morphologies. They present a striation orientation parallel to their a-axis (Fig. 5d), although two orientations are also observed. At CSM, only JRIVG-derived clasts are found, while at MH erratic lithologies are found along with reworked marine shells fragments (Fig. 7c). The light-brown matrix shows a strong subhorizontal and subvertical penetrative fracturing and usually has a "hardened" aspect. In thin section, a complete predominance of basaltic components was identified. When overlying lava flows (Ft), striated tops are observed. "Squeeze-up" structures are also recognizable, with upward injections of diamictite matrix into the overlying pillow lavas (Fp) and hyaloclastite breccias (Bpm).	Lodgement till, deposited by a locally wet-based sliding glacier, in a polythermal regime.
Foreset-bedded diamictite and conglomerate	D–Cs	150	MH	Weakly- to moderate-bedded, matrix- to clast-supported, diamictite (clast content <25%) and clast-rich (up to 85%) conglomerate. Beds are massive to normal graded and up to 15 m thick. Form steeply dipping foreset sequences (Fig. 7a). Stratification is mostly planar, although asymptotic stratification is also observed. Basalt is the most abundant clast lithology (more than 90% of the clast population). However, granite, schist, gneiss and sandstone erratic clasts are also observed. Clasts are facetted and rarely striated. The matrix is sandy to gravelly, mostly composed of basaltic fragments and minor epiclastic material (erratic).	Subaqueous fans formed by high-density debris flows, in a very proximal glaciomarine environment, probably deposited near the grounding-line of a floating glacier (ice shelf).

Table 1 (*continued*)

Lithofacies	Code	Thickness (m)	Locality	Description	Interpretation
Mudstone and siltstone	Ms	25	MH	Rhythmically and well-laminated mudstone and minor siltstone. Each bed is internally massive and between 1 and 5 cm thick, alternating between dark green mudstone layers to thicker, light green siltstone layers. Lamination is planar and subhorizontal usually disturbed by dropstones (Fig. 7b). This lithofacies is intimately related with diamictites (Dw). In thin section, component recognition is difficult given its fine grain size.	Very quiet, layer-by-layer deposition of fine particles by suspension or low density turbidity currents (distal glaciomarine setting). The presence of dropstones probably indicates ice-free sea and deposition from thawing icebergs (ice-rafted debris).
Stratified sandstone	Ss	12	MH	Yellow tuffaceous sandstone, thinly- to mediumly-bedded and moderately- to well-sorted (Fig. 7a). Internal bed structure includes wavy to planar lamination and normal grading. Main components include coarse to medium volcanic sand grains, including glassy to holocrystalline basaltic lithoclasts, though isolated quartz grains and erratic lithoclasts are also present. Bed contacts are always sharp and include erosive bases, with channel-like erosive scours, filled with gravelly sandstones (chute-and fill structure). Highly fragmented marine shells are observed.	Turbulent flow, either as subglacial streams, where water supply is usually continuous on wet-based glaciers, or as ice-proximal concentrated density currents (bottomset delta facies), in a medium to distal ice-proximity.

trigonometric methods (with clinometer, telemeter, measuring tape), description of bed contacts, geometry, lateral continuity, sedimentary structures, and clast characteristics. When possible, clast fabrics were measured in the diamictites together with the direction of striated pavements. The seventeen recognized lithofacies are briefly described and interpreted in Table 1, together with more detailed descriptions in the electronic Supplementary material. Coherent volcanic facies, especially lava flows, were sampled for unspiked K–Ar dating. Details on sampling sites and analytical methods related to K–Ar dating can be found in the electronic Supplementary material, as well.

4. Results

4.1. Volcanic stratigraphy in the Cerro Santa Marta area

The region here informally referred to as the Cerro Santa Marta area is located in the northwestern portion (Fig. 2) of James Ross Island. Here, two major unconformities of glacial origin separate two eruptive unit complexes to which we simply refer as Unit 1 and Unit 2. The basal unconformity (U1 from now on) separates the Cretaceous bedrock and older JRIVG-related pillow breccias from the overlying Unit 1. The upper limit of Unit 1 is marked by the second glacial intravolcanic unconformity (U2), which gradually descends towards the south. The eruptive lithofacies lying above U2 are referred to as Unit 2. In the following sections, we describe how the recognized lithofacies (Table 1) are vertically and laterally arranged in Cerro Santa Marta and Massey Heights. This arrangement, together with unit correlation and the altitude variation of the main unconformities, is shown on the stratigraphic logs in Fig. 3. Further details on each log can be found in the electronic Supplementary material.

4.1.1. Cerro Santa Marta (CSM)

Cerro Santa Marta (also referred to as Smellie Peak, CSM from now on) is located ~4 km west of Santa Martha cove and 4 km south of the southern edge of Lachman Crags (Fig. 1). For CSM, previously reported $^{40}Ar/^{39}Ar$ ages range from ~5.9 to ~5.1 Ma (Kristjánsson et al., 2005). East of CSM, across a region exceeding 10 km^2, several small volcanic hills reach Croft Bay's western shore (Fig. 2). These volcanic hills are rotational slide-blocks (Strelin and Malagnino, 1992), with sliding focused at contact with the relatively unconsolidated Cretaceous bedrock, which dips to the southeast at very low angles (~5°). This region of slide-blocks was also visited as it preserves important lithofacies not recognized or poorly exposed on *in-situ* outcrops.

4.1.1.1. Unit 1 at CSM. The U1 basal unconformity is not exposed at CSM but it is in fact well-exposed in the slide-block region, where it is carved to the Cretaceous bedrock and, in places, affecting an older JRIVG-pillow breccia unit (log 1 in Fig. 3) whose age is unknown. This undulating erosive surface is intimately related with a laterally-discontinuous, weakly-bedded diamictite (Dw), which closely resembles clear basal glacial lithofacies at Massey Heights (see below). Clast lithologies in this deposit show a predominance of JRIVG-derived clasts, but fewer erratic clasts of exotic lithologies (granites, low grade metamorphic rocks, altered acidic volcanics) derived from the Antarctic Peninsula (e.g., Aitkenhead, 1975) are also present (Fig. 5a). Within this diamictite there are relatively unconsolidated gravelly-sand lenses (Fig. 5b), with rounded pebbles and well-sorted sand which we infer were deposited as glaciofluvial sediments in subglacial streams. At CSM's west face, the contact between the Cretaceous bedrock and the overlying Unit 1 volcanics is covered by scree. At ~450 m above sea level (m a.s.l. from now on), ~100 m thick foreset-bedded pillow breccias (Bpw) are laterally continuous for more than 1.5 km. Foreset beds dip towards the south, suggesting that the source of these hyaloclastite breccias must have been located somewhere north of CSM. At 560 m a.s.l., subhorizontal, pāhoehoe-type lava flows (Ft) overlie the foreset-bedded pillow breccias and this contact is, as mentioned, referred to as the passage zone. In the case of CSM, between lava flows close to the passage zone, thin layers (<2 m) of palagonitized massive hyaloclastite (Bpm) are found interbedded, suggesting that these lavas may have flowed underwater for some distance while maintaining their coherent nature. In the upper part of the pāhoehoe lava pile, no such interbedded hyaloclastite breccias are observed. Overlying these lava flows, scoriaceous lapilli and bomb deposits (L–Bw) form a characteristic "red band" across CSM's northern face (Figs. 4 and 5d). This deposit is >30 m thick and it dips mainly to the southeast. Large spindle bombs (Fig. 5d) and spatter deposits indicate close proximity to the volcanic vent. We interpret these lithofacies as products of alternating subaerial strombolian- and hawaiian-type eruptions, which probably constructed a cinder cone on the surface. Dip values (between 12 and 30°) suggest that only external flank cones are preserved and that the vent region was located not far to the north (Fig. 4b). This provides strong evidence that CSM was the source of at least some of the eruptions. A second package of pāhoehoe-type compound lava flows overlies the southern flank of the cinder cone remnants (Fig. 4), and we infer that these lava flows were emitted from the cinder cone itself. In places, fragments (between 1 and 5 m) of red bedded scoria are found between the lava flow units, which we interpret as rafted blocks along a lava flow during a stage of scoria cone collapse (Sumner, 1998). At the south end of CSM (log 4 in Fig. 3), a thick (~45 m) lithic megabreccia

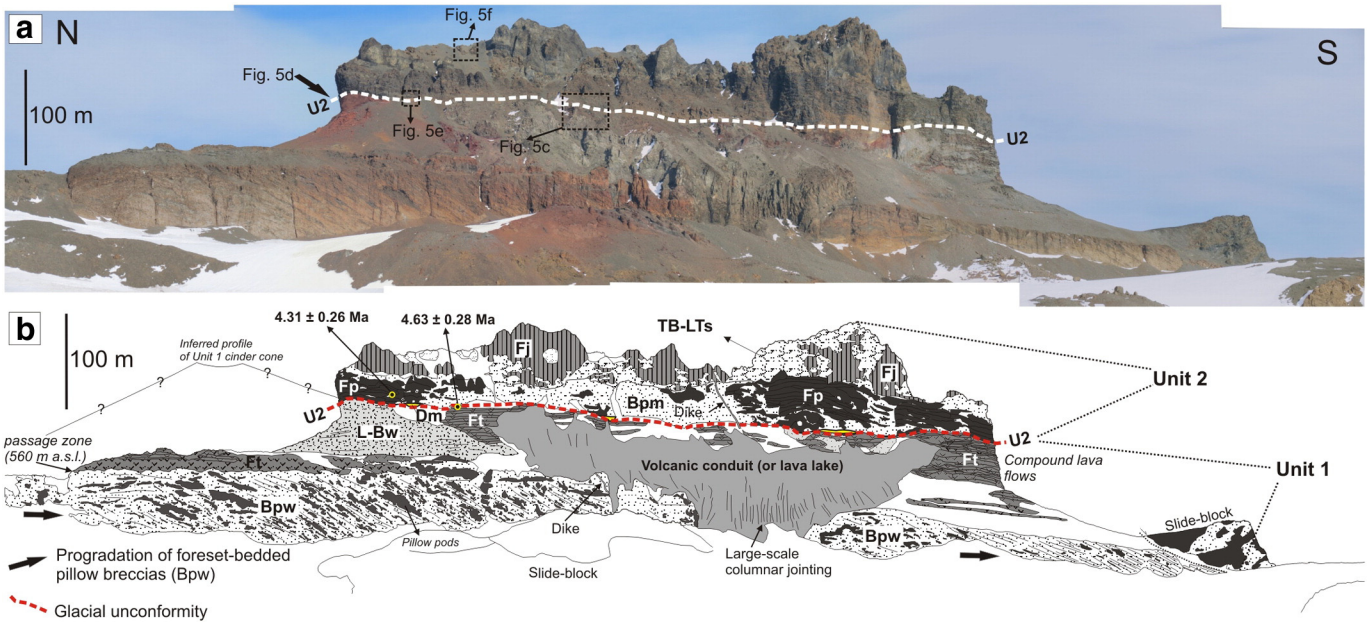

Fig. 4. Panoramic view of CSM's west face as seen from IJR-45 Glacier. a. The section is 300 m high and 1.5 km long. White dashed line indicates U2 unconformity. b. Interpretative sketch showing sites of dated samples, progradation of Unit 1 foreset hyaloclastite beds, U2 unconformity (red dashed line) and related diamictites (Dm, yellow patches). U1 unconformity is inferred to truncate Cretaceous bedrock which is covered by scree. Note the large dolerite body intruding older eruptive units (Unit 1), which can be interpreted as remnant of a volcanic conduit or lava lake. See also the highly irregular contacts between columnar-jointed basalts (Fj) and TB-LTs lithofacies. Also we present a speculative paleo-profile of Unit 1 cinder cone, based on scoria bed (L–Bw) dips; the beds are interpreted as former external cone flanks. (For interpretation of the references to color in this figure legend, the reader is referred to the web version of this article.)

deposit (MB) crops out, with large (up to 2 m) basaltic clasts indistinguishable from the subaerial lava flows and intensely intruded by small and irregular basaltic bodies. As evidence for water interaction is almost lacking (e.g., no palagonite alteration), we suggest that this megabreccia deposition is related to subaerial large-scale collapses of the lava flows, most likely due to gravitational instabilities in the volcano flank probably associated with dike injections (e.g., Elsworth and Voight, 1995).

On the west face, a large dolerite body (part of lithofacies P) (Figs. 4 and 5c) intrudes all Unit 1 lithofacies. This intrusive is approximately 270 m high and it has a gross lopolith-like morphology, with a narrow (~50 m) massive dike-like lower section and development of large-scale (between 0.5 and 2 m in diameter) vertical columnar jointing, changing upwards to a laterally spread (~300 m), dish-like more vesiculated body (Fig. 4) where columnar jointing, although less obvious, is not vertical but oblique and sometimes parallel to the contact with the host-rock. This contact (mainly against foreset-bedded pillow breccias and tabular lava flows, Figs. 4 and 5c) is irregular and in places, thin (~1 m) dikes are observed extending out of the main body. Near the contact, thermal modification of the host-rock is evident as color modification, specifically a reddish alteration of the palagonitized hyaloclastites. The morphology of this intrusion resembles shallow dike–sill complexes such as those studied in the Neogene basaltic rocks from Hungary by Németh and Martin (2007) and interpreted by them as feeding volcanic systems of phreatomagmatic volcanoes, probably emplaced at depths in the order of 50–100 m below the surface. On the other hand, the dish-like morphology and the development of large-scale vertical columnar jointing are also typical of fossilized lava lakes, such as those exposed at crater walls of several basaltic volcanoes (e.g., Vanuatu, see Németh and Cronin, 2008). Whatever the case, we believe that the emplacement level of this intrusive must have been very shallow (probably <200 m), further supported by the fact that it intrudes subaerial lava flows and it is highly vesicular in upper sections. The orientation of the columnar joints may be taken as an indicator of magma flow direction in the intrusive, changing from vertical in the lower section to more horizontal in the upper levels.

Unfortunately, there are no radiometric ages for this intrusion in order to correlate it with Unit 1 or 2. However, we infer that it is related to Unit 1 for two reasons. Firstly, there are no contact relationships of any kind with Unit 2 (i.e., Unit 2 volcanics were deposited after the volcanic conduit was formed), and secondly, this body is never found above 620 m a.s.l., the elevation of the U2 unconformity. This suggests that it was erosionally truncated together with subaerial lava flows from Unit 1 (see Fig. 5b). Overall, we conclude that this intrusive body is the remnant of a shallow volcanic conduit (or lava lake) centered at CSM, feeding a volcanic apparatus on a surface now removed by erosion. In this scenario, this conduit was most likely the source of cinder cone deposits located slightly north (Fig. 4) as well as lava-fed delta systems assigned to Unit 1, now exposed along Massey Heights (see below).

4.1.1.2. Unit 2 at CSM. As mentioned above, U2 unconformity is found at a constant altitude of ~620 m a.s.l. and is overlain by a massive diamictite (Dm) (Fig. 5e), which is here interpreted as a lodgement till resting on a glacially-abraded surface carved on subaerial lava flows (Ft) and cinder cone deposits (L–Bw) from Unit 1 (Fig. 5d). The clast fabric of this massive diamictite has a strong a-axis SW–NE orientation (see bi-dimensional rose diagram from twenty five basaltic clasts measured, Fig. 3) which is highly coincident with a N38° striation orientation measured on top of glacially-abraded lava flows from Unit 1, thus giving the orientation of paleo-ice flow (SW–NE).

After the formation of the U2 unconformity, Unit 2 volcanics were formed and locally rest on glacial deposits (Fig. 5e) whereas in other places, where the glacial diamictite is not present, either due to non-deposition or erosion, volcanic lithofacies rest directly over tabular lava flows (Ft) or scoriaceous deposits of the L–Bw lithofacies (Fig. 5d) ascribed to Unit 1. Pillow lavas (Fp) form the earliest eruptive products of Unit 2. Where they overlie massive diamictites (Dm) the contact between them is sharp and in places, there are upward injections of diamictite into the overlying pillow lavas. These structures were described by Hambrey and Smellie (2006) as "squeeze-up" structures and they indicate that these diamictites were relatively soft and unconsolidated diamicton when pillow lava extrusion occurred, thus a short

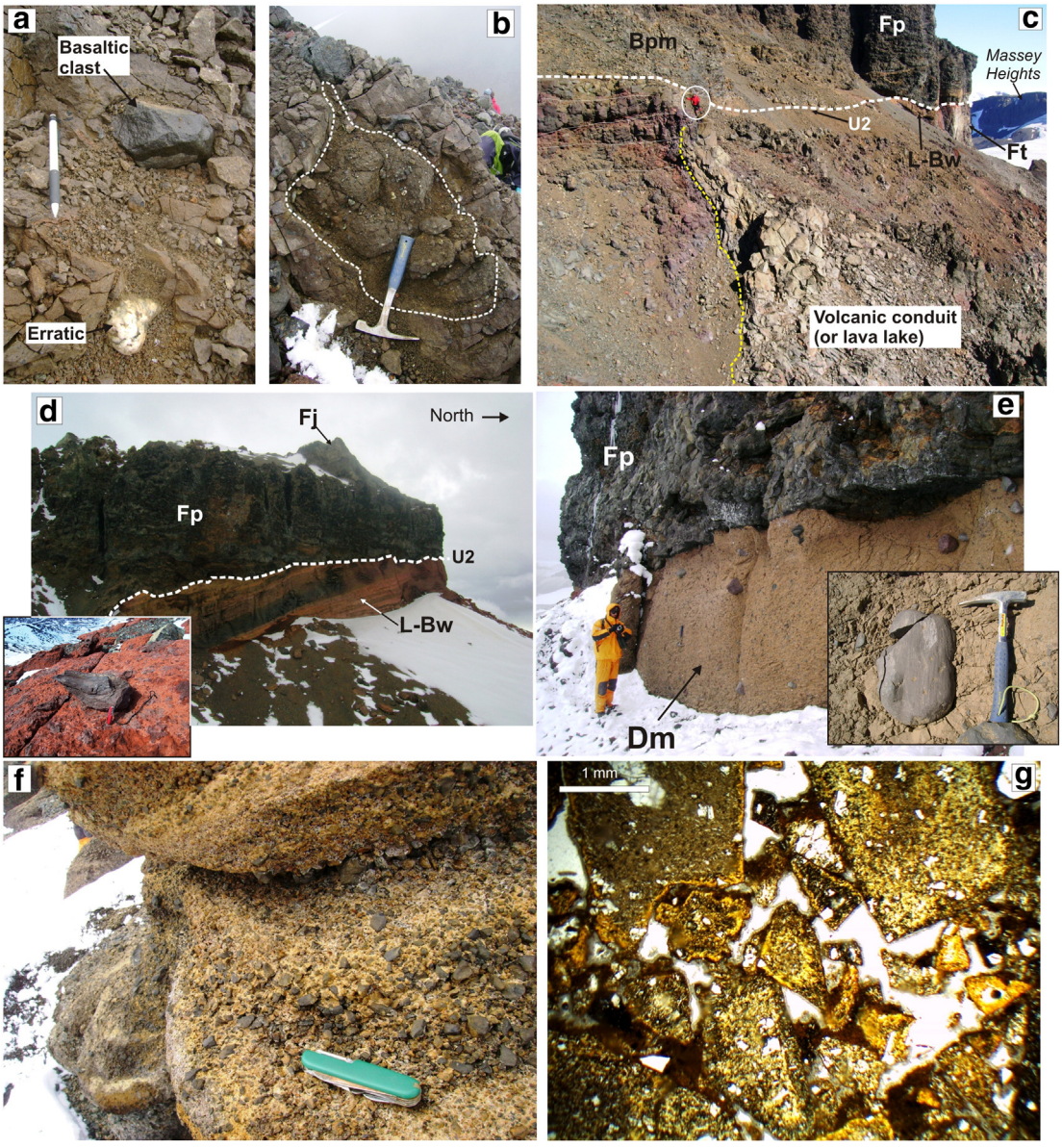

Fig. 5. Field photos and photomicrographs of lithofacies from CSM. a. Erratic (injected schist) and facetted basaltic clast included in a weakly-bedded diamictite (Dw) related to U1 unconformity. Pencil for scale. b. Outlined gravelly-sand lense included in the same diamictite as photo a. Hammer for scale. c. Subvertical intrusive contact (dashed yellow line) between the main volcanic conduit/lava lake and subhorizontal reddish lava flows (Ft) from Unit 1. A few meters above, U2 unconformity and overlying subaqueous lithofacies (Bpm and Fp) of Unit 2 are indicated. Person for scale (white circle). d. CSM's northeast face. Moderately-bedded red scoriaceous lapilli and bomb deposit (lithofacies L–Bw) from Unit 1, dipping southeast (inset photo: loose spindle-shaped bomb. Pocket knife for scale). The upper contact (white dashed line) is U2 unconformity and directly underlies the northern pillow lava (Fp) mound of Unit 2. Columnar-jointed lavas (Fj) are observed in upper levels. Section is ca. 30 m high. e. 2.5 m thick, massive clast-poor diamictite (Dm) related to U2 unconformity, at 620 m a.s.l. Clasts, usually facetted and striated, are only basaltic and JRIVG-derived (insep photo, hammer for scale). Overlying this diamictite above a sharp contact are pillow lavas (Fp) of Unit 2. Person for scale. f. Lapilli tuff beds (TB–LTs) of Unit 2 show diffuse stratification, normal grading and clast-supported fabric. Pocket knife for scale. g. Photomicrograph from a lapilli tuff (TB–LTs) of Unit 2 (same outcrop as photo e). Note blocky and equant, weakly-vesiculated vitroclasts, and intense palagonitization on vitroclast edges. (For interpretation of the references to color in this figure legend, the reader is referred to the web version of this article.)

time span elapsed between deposition of the two units. Two well-developed pillow mounds are observed at the southern and northern exposures in CSM, both reaching more than 70 m thick (Figs. 4 and 5d). Each pillow mound is characterized by vertical stacking of individual pillow lobes whose thickness ranges between 0.5 and 8 m, and up to 150 m long. Pillow lavas grade, both laterally and upwards, to massive pillow breccias (Bpm). These pillow breccias usually have a chaotic architecture, although foreset-bedded layers are discernible in places, dipping south. Up section, these pillow breccias grade into poorly-bedded tuff breccias and lapilli tuffs (TB–LTs). This lithofacies is characterized by palagonitized massive tuff breccia layers, in which pillow fragments are still identifiable, and lapilli tuff beds that locally show normal grading (Fig. 5f). Thin sections of the lapilli tuff matrix (Fig. 5g) show the predominance of juvenile, poorly-vesicular vitroclasts with blocky, equant morphologies. An upward decrease in grain size from pillow breccias to lapilli tuff beds reflects a more efficient fragmentation process due to decreasing hydrostatic pressure. However, equant and blocky vitroclast shapes may be produced by explosive interaction between magma and water (e.g., Type 1 pyroclasts of Wohletz, 1983) or they can be formed as the result of largely non-explosive cooling–contraction granulation processes (e.g., Maicher et al., 2000). Previous Unit 2 lithofacies are intruded and in parts covered by highly irregular and thick columnar-jointed basalts (Fj), which were fed by thin (<1 m) subvertical dikes. These columnar-jointed basalts have features that suggest that they were emplaced in a subaqueous setting (Fig. 4), such as the presence of a carapace of palagonitized

breccias (similar to massive tuff breccia beds of TB–LTs lithofacies), the chaotic development of entablature-type columnar jointing and their highly irregular contacts with TB–LTs lithofacies (e.g., Edwards et al., 2002). This last feature suggests a "wet" host rock and a short time between TB–LTs lithofacies subaqueous deposition and columnar-jointed basalt emplacement.

Overall, the subaqueous lithofacies of Unit 2 are >120 m thick and, thus the approximate depth of the water body at the time eruptions took place. In a slightly displaced block at CSM's southeast face (log 4 in Fig. 3), columnar-jointed basalts (Fj) are covered by a thin package of tabular lava flows (Ft) with ropy textures on their tops and reddish oxidized scoriaceous bases, suggesting subaerial effusion during the last phases of volcanic activity during Unit 2 emplacement. The contact between purely subaqueous and subaerial lava flows can be also considered a passage zone and is located here at ~680 m a.s.l.

4.1.2. Massey Heights (MH)

A few km southwest of CSM, a 5 km-long elongated ridge is referred to as Lookalike Peaks (highest points) in the north, Stickle Ridge in the central portion, and Massey Heights in the south (Fig. 2). For convenience, we refer to the entire ridge and both peaks as Massey Heights (MH from now on). The volcanic succession is ~500 m thick and the exposures are excellent given vertical rock faces. Published age constraints indicate that the eruptive units exposed at MH were deposited between ~6.2 and ~4.4 Ma (Sykes, 1988; Kristjánsson et al., 2005). Meseta de las Lagunitas (Fig. 2) is a slide-block region, similar to those mentioned for CSM's eastern side, from where two logs are shown in Fig. 3.

4.1.2.1. Unit 1 at MH. Unit 1 at MH encompass more than 200 m of volcano and epiclastic strata, starting at its base with glacial lithofacies unconformably (U1 unconformity) overlying the Cretaceous bedrock at ~300 m a.s.l. (Fig. 6a). From north to south, the glacial lithofacies (Fig. 3) change. In the northern sections (logs 5 to 9, Fig. 3), weakly-bedded diamictite (Dw) with glacial erratics and rhythmically laminated mudstones (Ms) locally bearing dropstones predominate. Further south (Fig. 7a and log 10 in Fig. 3), the same laminated mudstones (Fig. 7b) are covered by stratified tuffaceous sandstones (Ss) which bear highly fragmented marine shells. These sandstones show several structures (lenticular beds, cross-bedding) that imply a high-energy depositional regime. Overlying both lithofacies are foreset-bedded diamictites and conglomerates (D–Cs), which include both JRIVG-derived basaltic clasts and erratic lithologies, and form a ~100 m thick sequence that can be traced for several kilometers. The presence of marine shell fragments within the lower sequence provides important evidence for glaciomarine deposition conditions.

Laterally discontinuous pyroclastic lithofacies, more than 40 m thick, formed by planar- and cross-bedded tuffs and minor lapilli tuffs (Tsc) cover the glacial strata, especially in the northern exposures, and

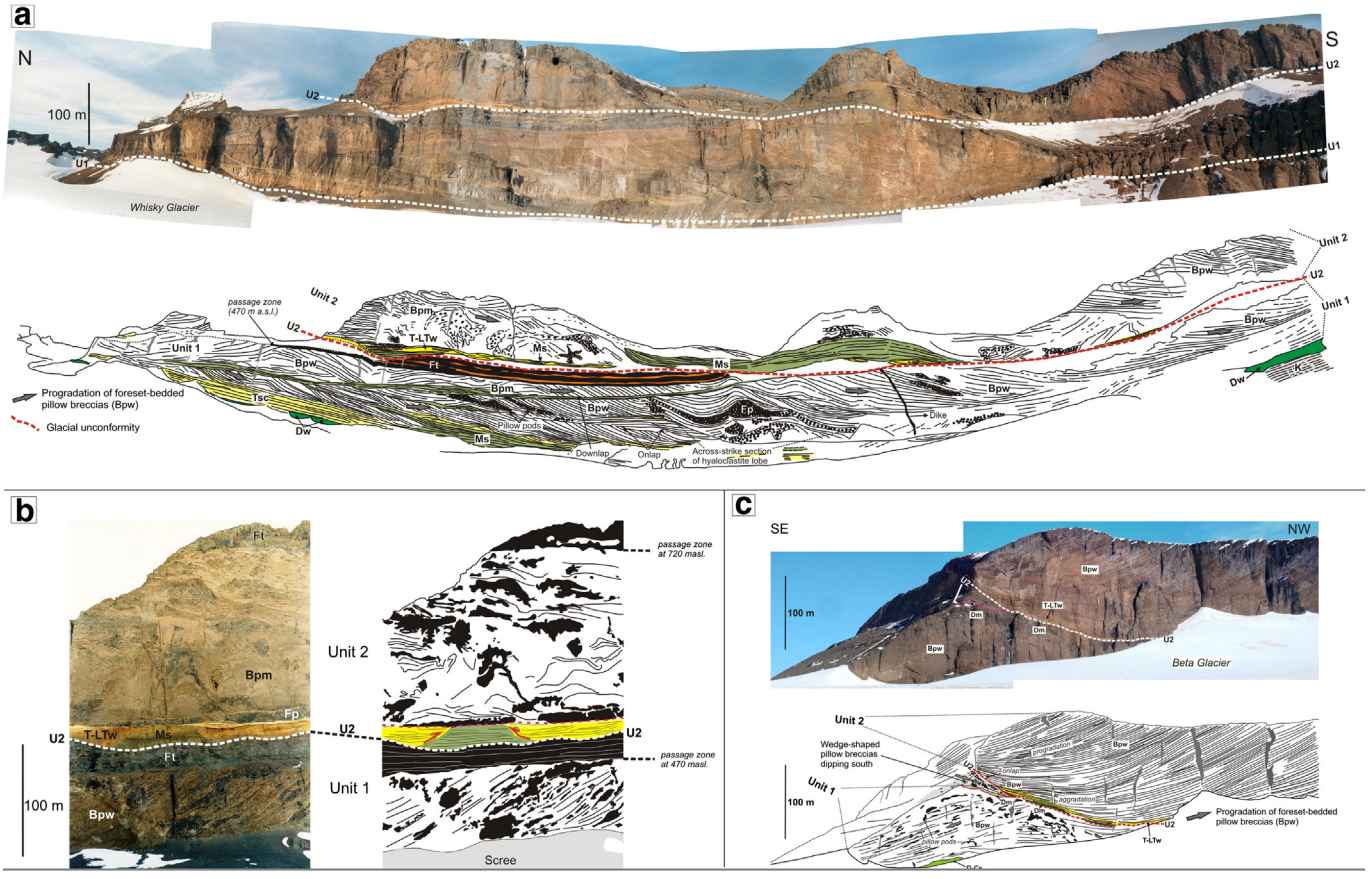

Fig. 6. West face of MH, as seen from Whisky Glacier. The section is ~2.5 km long and >200 m high. Glacial deposits related to U1 unconformity are shown in dark green (Dw lithofacies), Tsc lithofacies is shown in light yellow, Ms lithofacies in light green and T–LTw lithofacies in dark yellow. Unit 1 lava flows (Ft) are shown in black, together with hyaloclastite layers (in orange) separating each lava flow. b. North face of MH. The rock face is ~250 m high. Overlying U2 unconformity, a complex faulted contact can be observed between lithofacies Ms and T–LTw, probably as a product of load deformation of the overlying thick (~100 m) package of massive pillow breccias (Bpm), with a chaotic (slumped) architecture. Passage zones of Unit 1 (at 470 m a.s.l.) and Unit 2 (at 720 m a.s.l.) are indicated. c. Southeast face of MH as seen from Beta Glacier, where U2 unconformity is represented by two different intravolcanic glacial levels: a lower one (pink dashed line) which is a massive diamictite (Dm), bearing highly-fragmented marine shells and erratic clasts, and an upper diamictite (Dm, green-colored) lacking fossil fragments and erratic clasts, and resting on a concave erosive surface (white dashed line). Tuffs and lapilli tuffs (T–LTw lithofacies, yellow-colored in the lower figure) and foreset-bedded pillow breccias (Bpw) of Unit 2 overlie this diamictite. See text for further explanations. (For interpretation of the references to color in this figure legend, the reader is referred to the web version of this article.)

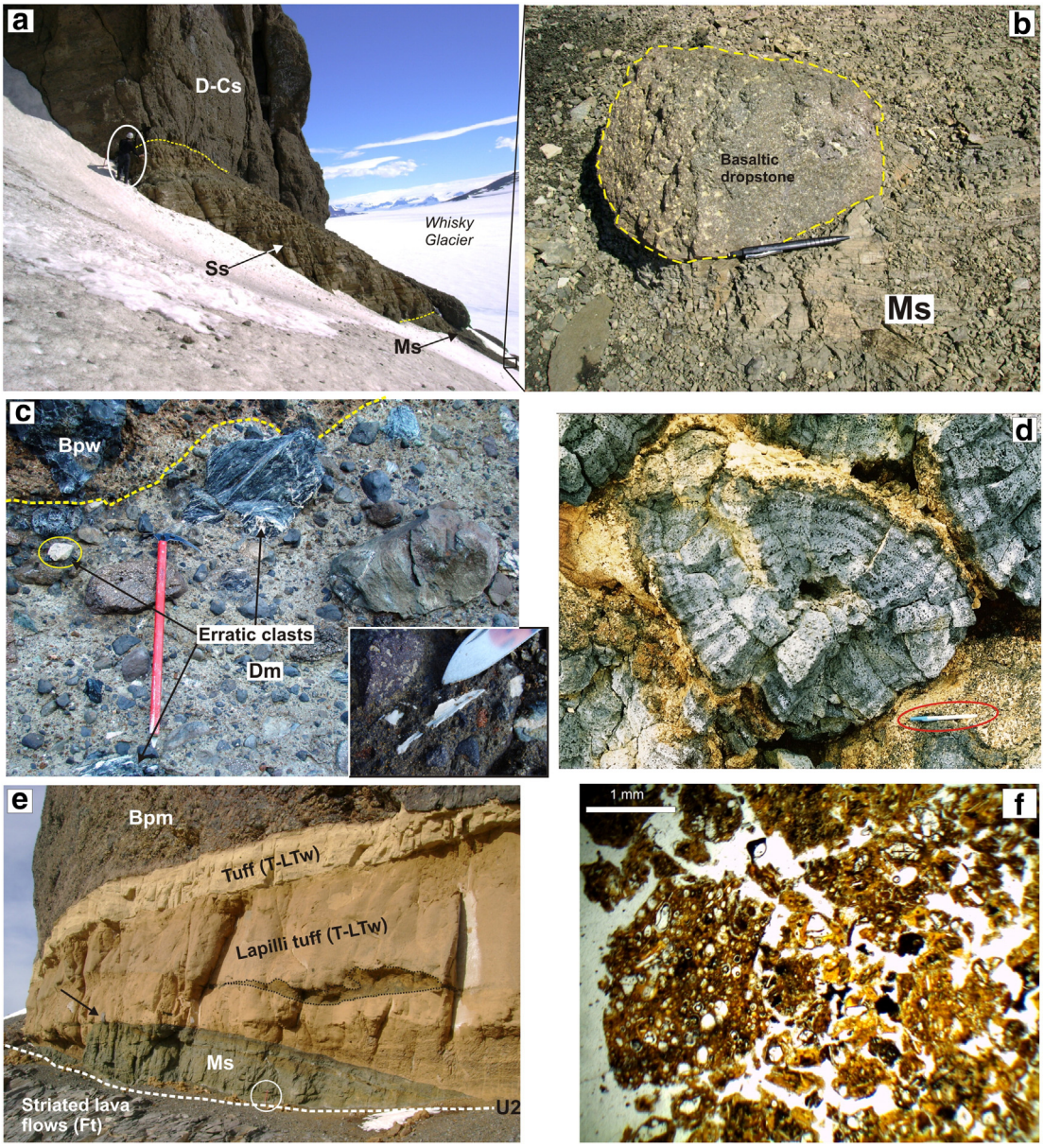

Fig. 7. Field photos and photomicrographs of lithofacies from MH. a. West face of MH. Glacial strata related to U1 unconformity, each one separated by a yellow dashed line. At the base, laminated mudstones (Ms) with dropstones underlie well-bedded tuffaceous sandstones (Ss), which bear highly-fragmented marine shells. The upper unit are foreset-bedded diamictites and conglomerates (D–Cs) dipping south. Person for scale (white circle). b. A ~30 cm vesicular basaltic dropstone (outlined) disturbs the fine lamination of Ms lithofacies. Pencil (15 cm) for scale. c. Southern end of MH. Massive intravolcanic diamictite (Dm, lower level) related to U2 unconformity covered by wedge-like deposit of pillow breccias (Bpw). Near the upper contact, abundant marine fossil fragments were found (inset photo: pectinid? fragment). Note the presence of erratic clasts, mainly low grade metamorphic rocks and whitish plutonic rocks (yellow circle). Ice axe (70 cm) for scale. d. Complete pillow from foreset-bedded pillow breccias (Bpw) of Unit 1, with concentric vesicular pattern. The inter-pillow material is formed by palagonitized hyaloclastite. Pencil (15 cm) for scale (red circle). e. Northern face of MH. Striated lava flows (U2 unconformity, white dashed line) underlie a lenticular deposit of laminated mudstones (lithofacies Ms) which is covered (and incorporated as lenses highlighted by a black dotted line) by ~9 m thick massive to weakly-bedded tuffs and lapilli tuffs (T–LTw). A sharp contact separates this lithofacies from the overlying pillow breccias (Bpm). Black arrow indicates a striated basaltic clast incorporated in T–LTw lithofacies. Ice axe (70 cm) for scale (white circle). f. Photomicrograph of a tuff sample (lithofacies T–LTw). Note highly-vesiculated and palagonitized vitroclasts. (For interpretation of the references to color in this figure legend, the reader is referred to the web version of this article.)

gradually disappear to the south, where the glacial deposits are covered either by foreset-bedded pillow breccias (Bpw) or by Unit 2 lithofacies (Fig. 3). This lithofacies shows diverse sedimentary structures, ranging from large-scale planar- and cross-bedding to centimeter-scale B-type climbing ripples, which indicates that pyroclasts were deposited at high aggradation rates, typical of high-density turbidity flows (Lowe, 1982). Thin section analysis of this lithofacies shows the predominance of juvenile vitroclasts with blocky and equant morphologies, similar to TB–LTs lithofacies (see Table 1), which may suggest that the fragmentation process was largely non-explosive. Laterally, this lithofacies represents an equivalent of foreset-bedded hyaloclastite breccias (Bpw) which suggests a distal position within the lava-fed delta system. Unit 1 continues with ~120 m thick foreset-bedded pillow breccias (Bpw) that can be traced laterally for more than 5 km. Each breccia clinoform package is unconformity-bounded and show variable dips (usually >15°) to the south and southeast. Downlap stratal terminations are more common and usually related to normal or forced regressions (e.g., Catuneanu, 2002), which may result from lava-fed delta progradation and basinward retreat of the shoreline. Onlap basal terminations are also observed (Fig. 6a) and could indicate a transgression

event (i.e., creation of new accommodation space). Moreover, retrogradational stacking patterns are evidenced by distal, deeper-water laminated mudstones (Ms) overlying proximal foreset-bedded pillow breccias. This arrangement implies a change in the base level and a landward shift of the shoreline (i.e., transgression).

In places, foreset-bedded layers change to double-dipping, hummocky-like layer geometries, especially in the central section of MH's west face (Fig. 6a). These are interpreted as cross-strike sections of the hyaloclastite clinoforms, unlike the foreset-bedded layers, which represent along- or close along-strike sections. These changes in breccia bed architecture may be caused by shifting of the lava entry point, which could be a result of magma supply rate or coastline morphology, as schematized by Watton et al. (2013). Compound pāhoehoe lava flows (Ft), reaching more than 30 m thick, cover the foreset-bedded pillow breccias (Bpw) with a passage zone located at ~470 m a.s.l. The lava flows usually have pillowed and glassy margins, and are interbedded with thin (1–2 m) massive hyaloclastite (Bpm), suggesting that the pāhoehoe-type lavas flowed underwater for some distance, probably as lava tubes flowing over a gentle slope, which may have coalesced forming sheet flows (e.g., Umino et al., 2000), or even make their way onto the foreset, forming hyaloclastite, lava rags (pillow pods in Fig. 6a) and pillow debris (e.g., White, 2000). Lava fragmentation is mostly related to non-explosive processes (mainly thermal granulation and spalling), promoted as well with a slope increase, although explosive interaction, such as littoral explosions (Mattox and Mangan, 1997) cannot be discarded. The basaltic clast products of lava fragmentation were likely deposited as density currents (e.g., White, 2000; Skilling, 2002), forming a loose subaqueous debris slope (breccia clinoforms) which continuously built the delta front. Rarely, between each package of pillow breccias, we recognized volcaniclastic conglomerates, composed of pillow fragments within a gray-colored matrix and rare occurrence of erratic clasts. These conglomerates may be deposited as subaqueous mass-flow remobilization of the breccia clinoforms. Unit 1 is intruded by thin, irregular and subvertical dikes, whereas ellipsoidal intrusive rocks are found at the contact with the Cretaceous bedrock. It is plausible that these intrusives were also involved in delta construction as lateral feeders, but this needs to be tested.

At the southern end of MH (Fig. 6c; see also log 11 in Fig. 3), unlike the intravolcanic glacial level described in CSM, two glacial deposits are here related to U2 unconformity. The lower glacial level overlies a ~100 m thick package of Unit 1 foreset-bedded pillow breccias (Bpw). This level is a 9 m thick massive diamictite (Dm), which bears a large proportion of erratic boulders derived from the Antarctic Peninsula (Fig. 7c) and is herein interpreted as subglacial (lodgement) till. In addition, highly-fragmented marine shells are also found (Fig. 7c), such as pectinids and incrusting bryozoans. The presence of shell fragments included in a massive glacial diamictite is controversial and not necessarily speaks for a glaciomarine origin, given that these shells could be reworked from older glaciomarine deposits (Smellie et al., 2006a). Between the lower and upper glacial levels, a wedge-like unit of poorly foreset-bedded hyaloclastite pillow breccias (Bpw) is exposed, which dips to the north (Fig. 6c), clearly different from the south-dipping foreset beds forming the bulk of the sequence. This dip change may be related to delta front remobilization, shifting of the lava entry points or even coastline parallel lava flow (see Watton et al., 2013 and references therein), which may produce changes in the breccia clinoform architecture. The upper glacial level lies on a concave surface and is represented by a massive diamictite (Dm) lacking erratic clasts and shell fragments, and covered by Unit 2 tuffaceous deposits (T–LTw lithofacies) and foreset-bedded pillow breccias (Bpw). The concave surface may be related to glacial erosion, later characterized by vertical aggradation and lateral progradation of the breccia clinoforms onlapping onto this surface.

4.1.2.2. Unit 2 at MH. The U2 unconformity is best represented at MH as glacially-abraded pavements, particularly well-developed on the tops of pāhoehoe lava flows (Ft). The altitude of this surface gradually decreases to the south, from 495 m a.s.l. to 350 m a.s.l. Striae orientation in northern exposures (see Fig. 2) presents mainly a N100° orientation, but a less developed orientation of N44° is also present. Immediately on top of this erosive surface, the first Unit 2 lithofacies show a complex arrangement, especially between T–LTw and Ms lithofacies. Ms lithofacies shows very poor lateral continuity, because it is highly deformed and usually found as lenses included in T–LTw lithofacies (Fig. 7e). Ms lithofacies interpretation (see Table 1) suggests that it was deposited as fine mud particles, leading to horizontal lamination in a very quiet sedimentary environment. Its greenish color could be related to relatively anoxic conditions. Fig. 6a shows that Ms lithofacies can be laterally related as distal equivalents of foreset-bedded pillow breccias (Bpw) of Unit 2, implying a genetic relationship between them. However, deposition related to a glacial system cannot be discarded, given that its stratigraphic position is similar to that of massive diamictites at CSM (both units are directly overlying U2 unconformity) and their relation with the underlying glacial pavements. Overlying this muddy lithofacies (Ms), a "yellow band" forms the middle section of MH and is here ascribed to T–LTw lithofacies, which is formed of poorly-bedded tephra containing a striated basaltic clast near its base (Fig. 7e). This lithofacies shows evidence of explosive phreatomagmatic eruptions (see Section 6.1.4), such as vitroclasts with variable vesicularity (Fig. 7f), but predominance of irregular, vesicle-bounded vitroclasts (Type 2 of Wohletz, 1983), which may indicate both magmatic fragmentation due to volatile exsolution and explosive magma–water fragmentation. Poor bedding indicates a continuous tephra deposition product of ascending vesiculated magma interacting with external water.

The stratigraphy at MH continues with foreset-bedded (Bpw) and massive (Bpm) pillow breccias, separated from each other by minor unconformities. Massive-subtype is more common in the northern sections (closer to CSM, Fig. 6b) whereas foreset-bedded subtype characterize the central and southern exposures. This package of pillow breccias underlies ~30 m of gently south-dipping lava flows (Ft, Fig. 6b). These flows show pillowed glassy margins and massive beds of hyaloclastite breccia intercalations, suggesting that they were probably subaerial and later flowed underwater for some distance, as mentioned for Unit 1. The entire package of foreset-bedded pillow breccias (Bpw) and their cap-rock of lava flows (Ft) defines another ~200 m thick, hyaloclastite lava-fed delta sequence, which prograded south during eruptions, as foreset-bed dips suggest. The passage zone is found at ~720 m a.s.l. in the northern section and rises up to ~800 m a.s.l. 1.5 km to the south (see logs 5 and 6 in Fig. 3), which translates in a rising angle of ~3°. Unfortunately, the lava cap-rock disappears towards the south, which makes the Unit 2 passage zone an overall ill-defined surface, and it is not possible to detect any passage zone height variation. Absence of the topset lava flows at MH's southern section, between 600 and 650 m a.s.l., may be related to the development of the present-day flat erosive surface carved on hyaloclastite breccias. The origin of this surface may be related to subsequent glacier advances (erratics are usually found on top of this surface) or to a marine/lacustrine abrasion platform.

5. K–Ar chronology and comparison with published ages

Four new whole-rock unspiked K–Ar ages are reported in Table 2. Sample preparation and analytical methods can be found in the electronic Supplementary material. Fresh basaltic samples were collected to provide new age constraints on eruptive activity during Unit 1 and 2 depositions, and to compare our age data with previously published ages from the same region. Also, it is worth noting that all the chronological data provide important insights regarding glacial event/s that occurred in close association with volcanic activity, especially the development of the intravolcanic glacial unconformity (U2).

Table 2
New unspiked K–Ar age results from Cerro Santa Marta and Massey Heights.

Location—unit	Sample no.	Lat (°S)	Long (°W)	K (wt.%)	^{40}Ar rad (10^{-8} cm^3 STP/g)	^{38}Ar/^{36}Ar	^{40}Ar/^{36}Ar initial[a] fractionated Ar assumed	Age (Ma)[b]	Air fraction (%)
CSM—Unit 1	2SM08	63.930	57.921	0.819 ± 0.041	14.72 ± 0.78	0.1871 ± 0.0012		**4.63 ± 0.28**	52.5
CSM—Unit 2	SM12	63.929	57.919	1.156 ± 0.058	19.4 ± 1.0	0.1879 ± 0.0013		**4.31 ± 0.26**	60.1
MH—Unit 1	3MAS06	63.936	57.975	1.023 ± 0.051	20.7 ± 1.1	0.1879 ± 0.0012		**5.21 ± 0.32**	44.7
MH—Unit 2	3MAS02	63.937	57.975	0.749 ± 0.037	12.9 ± 2.8	0.1903 ± 0.0014	303.3 ± 4.3	***4.4 ± 1.0***	93.5

[a] ^{40}Ar/^{36}Ar initial was estimated from the measured ^{38}Ar/^{36}Ar ratio, which was fractionated from the atmospheric value of 0.1880.
[b] ^{40}Ar/^{36}Ar initial = 296.0 is assumed. Error: 1σ.

5.1. Age of Unit 1 volcanics

Sample 2SM08 was collected at 617 m a.s.l. in CSM from a subaerially-emplaced lava flow which we infer was emitted from the cinder cone located less than 1 km to the north, at a similar level. This flow has a glacially-truncated top, covered by a glacial diamictite (U2 unconformity), so its age can be considered a maximum age for the glacial unit's deposition. This sample yielded an age of 4.63 ± 0.28 (error ± 1σ), which significantly differs from a ^{40}Ar/^{39}Ar age of 5.89 ± 0.09 Ma (Kristjánsson et al., 2005) for a lava flow also ascribed to Unit 1 but probably related to older flows emitted from an unrecognized vent located somewhere north of CSM. In this context, sample 2SM08 (early Pliocene) was emitted from CSM's cinder cone and its radiometric age can be considered as the beginning of eruptive activity centered at CSM.

Sample 3MAS06 was collected at MH from a tabular lava flow with signs of glacial erosion (U2 unconformity). Kristjánsson et al. (2005) previously dated by ^{40}Ar/^{39}Ar a single lava sample from Unit 1 which yielded a very good quality late Miocene age of 6.16 ± 0.08 Ma. Our unspiked K–Ar result yielded an age of 5.21 ± 0.32 Ma and the age difference may be due to sampling different lava flows (i.e., we sampled a younger one). We infer that the ~6.2 Ma lava is from an older Unit 1 lava-fed delta formation, while our ~5.2 Ma lava flow erupted from a younger vent centered at CSM, but associated with the same lava-fed delta system (Fig. 8). It is clear that more precise radiometric ages are needed to determine the volcanic evolution through time. Nevertheless, as we discuss in Section 6.1.2, these radiometric ages suggest that a geologically meaningful time span existed between the eruption of volcanic products from an unrecognized vent north of the study area (i.e., between 6.2 and 5.9 Ma) and the beginning of eruptive activity centered at CSM (5.2–4.6 Ma), therefore implying that an unrecognized unconformity must be present within Unit 1 sequence.

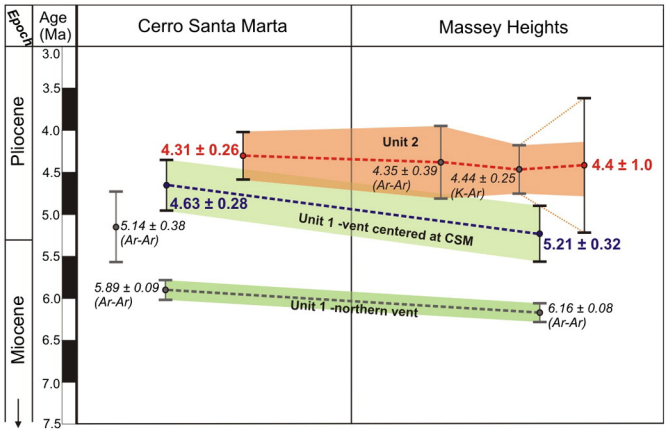

Fig. 8. Summary of published (black) and new (colored) radiometric ages for eruptive units described here from CSM and MH. Blue ages belong to Unit 1 and red ages to Unit 2. For ^{40}Ar/^{39}Ar ages (Kristjánsson et al., 2005) the error bars are ±2σ, whereas for K–Ar ages (both our ages and Sykes's (1988) age of 4.44 ± 0.25 Ma) they are ±1σ. Light green bars represent the two recognized periods (6.2–5.9 Ma and 5.2–4.6 Ma) of volcanic activity during Unit 1 deposition. Orange bar connects all the available ages of Unit 2. Correlation between these ages and 5.14 ± 0.38 Ma age, which we consider as an outlier, remains unsolved. (For interpretation of the references to color in this figure legend, the reader is referred to the web version of this article.)

5.2. Age of Unit 2 volcanics

Sample SM12 was collected at CSM from a pillow lava core resting on diamictites (U2 unconformity). Its radiometric age is 4.31 ± 0.26 Ma (early Pliocene), which is the minimum depositional age for U2-related diamictites. Kristjánsson et al. (2005) obtained a ^{40}Ar/^{39}Ar age of 5.91 ± 0.08 Ma (not shown in Fig. 8) for the same unit, which is inconsistent with our unspiked K–Ar age. Kristjánsson et al. (2005) also dated the columnar-jointed basalt (Fj lithofacies) unit at CSM's summit and obtained an age of 5.14 ± 0.38 Ma. Their stratigraphic position suggests that they should be younger or at least coeval with pillow lavas that yielded a K–Ar age of ~4.31 Ma. This contradiction remains unsolved. However, we can infer that Unit 2 volcanics were probably formed between .6 and 4.0 Ma.

Sample 3MAS02 was collected at MH. It corresponds to a hyalocrystalline pillow core from massive pillow breccias assigned to Unit 2. Unfortunately, the results indicate that this sample has probably suffered atmospheric Ar contamination and fractionation, as the high ^{40}Ar/^{36}Ar indicates. Nevertheless, our 4.4 ± 1.0 Ma age roughly agrees with the 4.35 ± 0.39 Ma age obtained by Kristjánsson et al. (2005) and the 4.44 ± 0.25 Ma K–Ar age reported by Sykes (1988), which all together confirm that Unit 2 volcanics were formed around 4.4 Ma (early Pliocene).

6. Discussion

6.1. Volcanic evolution of the JRIVG at Cerro Santa Marta area

According to our stratigraphic analysis and chronological data, we propose a volcanic evolution model of the JRIVG units in the Cerro Santa Marta area, together with a tentative correlation with analog units exposed at Lachman Crags.

6.1.1. Unconformity U1

As mentioned in previous sections, the oldest JRIVG units recognized around Cerro Santa Marta area show evidence of glacially-influenced deposition. The basement of these glacial lithofacies was either Cretaceous bedrock or pre-Unit 1 hyaloclastites, in which case volcanism was already ongoing during ice sheet expansions in the region. Nelson et al. (2009) postulated that this first glacial advance in the region occurred before ca. 6.2 Ma, based on the oldest volcanic units dated by Kristjánsson et al. (2005) which overlie the glacial deposits. It could be related to an Antarctic Peninsula ice sheet expansion between 7.2 and 6.6 Ma postulated by Grützner et al. (2005). The constant level of the Cretaceous bedrock at ~300 m a.s.l. suggests a low relief (i.e., relatively flat landscape) at the moment of ice sheet advance. Glacial lithofacies associated with the basal unconformity (U1) show signs of deposition in close association with a water body (Fig. 9a). In the proximal sector (close to the grounding line), the glacier deposited weakly-stratified

diamictites (Dw) and ice-proximal foreset-bedded diamictites and conglomerates (D–Cs), whereas in the distal parts deposited stratified sandstones (Ss) and rhythmically laminated mudstones and siltstones with dropstones (Ms). This lateral facies association is common within glaciomarine environments (e.g., Hambrey and McKelvey, 2000). In this sense, we agree with Nelson et al.'s (2009) conclusion that their foreset-bedded conglomerates (our D–Cs lithofacies) were deposited by subaqueous debris flows, probably forming an ice-contact underwater fan (Lønne, 1995) near the grounding-line of a marine-terminating glacier, probably a grounded tidewater glacier then floating as an ice

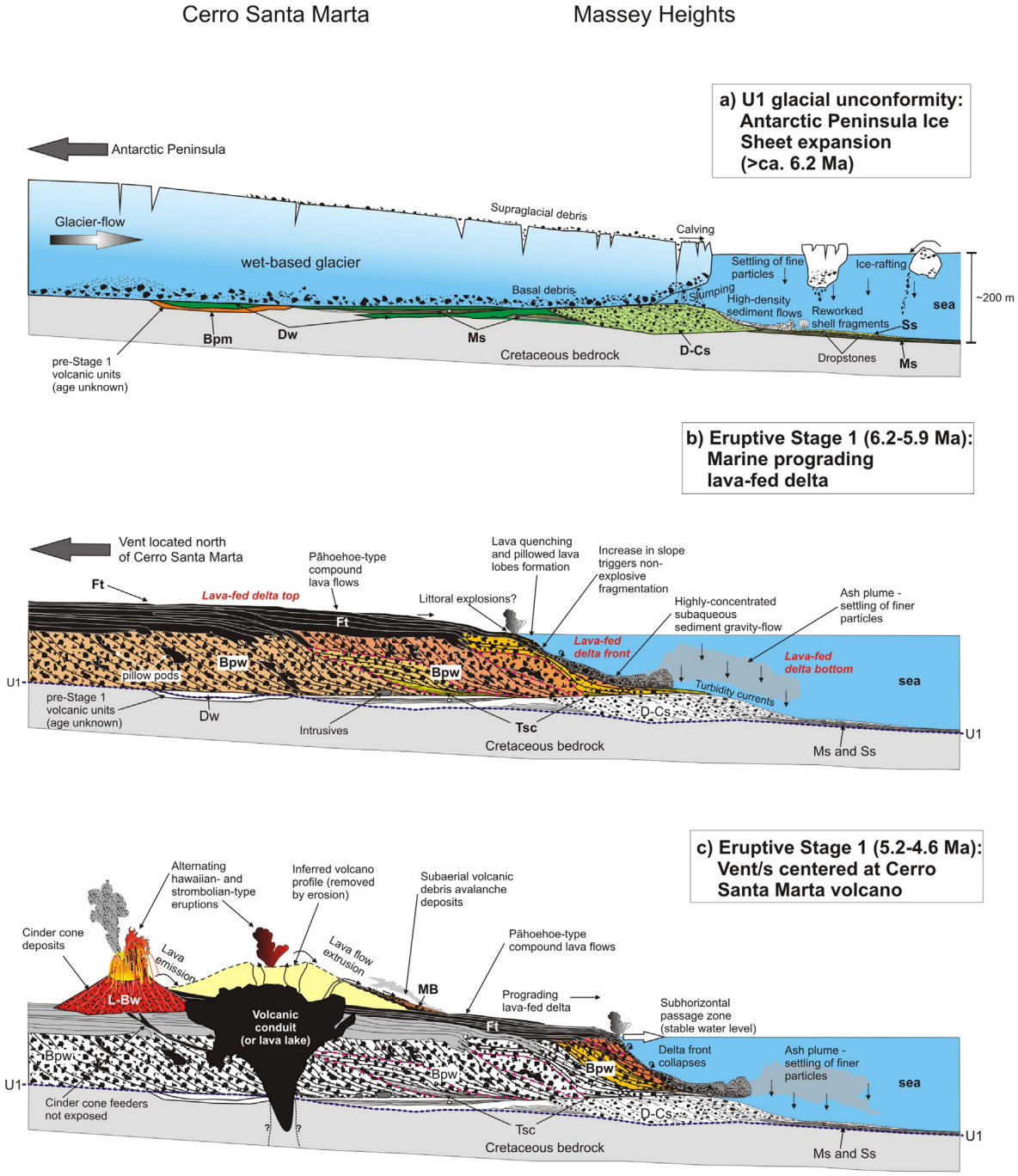

Fig. 9. Proposed schematic model showing the depositional environments and evolution of CSM and MH volcano and epiclastic succession (not to scale). Lithofacies are indicated by its corresponding code (see Table 1). a. U1 unconformity: Antarctic Peninsula ice sheet expansion sometimes before 6.2 Ma, eroding the Cretaceous bedrock and older JRIVG-units. Glacier probably floated over the sea (ice shelf) depositing submarine glacial deposits (Dw, D–Cs, Ss and Ms lithofacies) close to the grounding-line. b. Eruptive Stage 1: subaerial lava flow (Ft) emission from an unrecognized vent north of the study area. These lava flows formed a marine prograding lava-fed delta towards the south. c. Later, vent/s shifted to the north and centered at CSM. Subaerial lava flows, emitted from a cinder cone (L–Bw) and a larger volcanic apparatus above the main volcanic conduit/lava lake, continued feeding the same prograding hyaloclastite delta now exposed at MH. d. U2 unconformity (>4.6 Ma): a second glacial advance eroded previous units of Eruptive Stage 1. This glacier flowed from the W-SW and was probably a glacial tongue part of a James Ross Island-anchored ice cap. Coincident with glacier presence in the area, volcanism renewed during Eruptive Stage 2 mainly from CSM vents. Direct magma-ice interaction led to glacier base melting and formation a meltwater vault. e. Glacier roof collapse and formation of an ice-enclosed meltwater lake. Sub and supraglacial drainage combined with vertical growth of the volcanic pile led to shallowing of the water depth and onset of phreatomagmatic Surtseyan-type eruptions. f. Emergence of the englacial volcano and emplacement of a new prograding lava-fed delta system, forming a gently rising passage zone, most likely due to temporarily blockage of the subglacial drainage system and rising of the water level. Although not clear, we infer that this lava-fed delta also prograded towards the north forming the upper unit found at Lachman Crags. See text for further explanations.

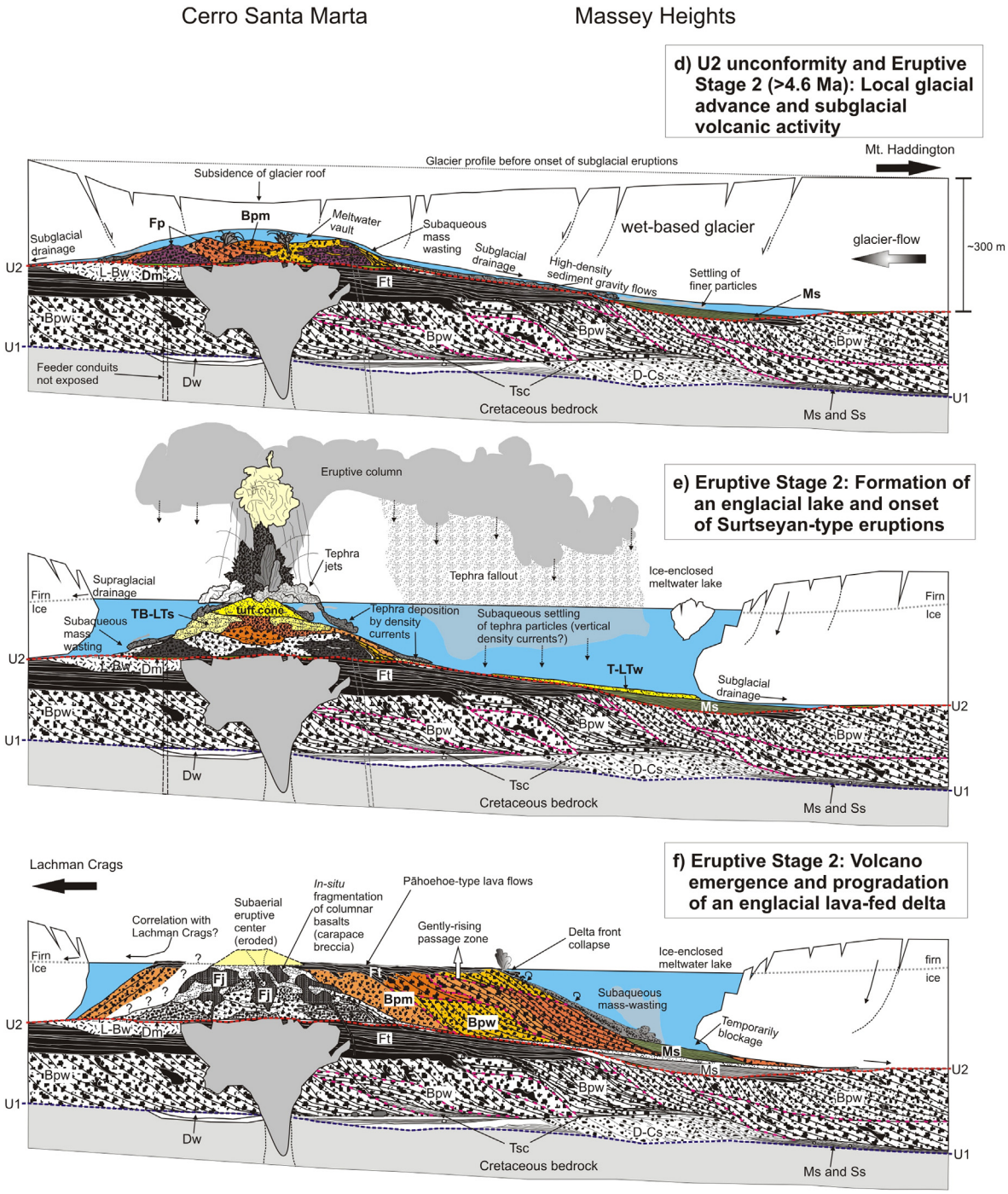

Fig. 9 (*continued*).

shelf. The presence of highly fragmented marine shell remains in sandstones (Ss lithofacies), which underlie foreset beds of D–Cs lithofacies also supports the idea of a glaciomarine environment. The ice sheet thermal regime must have been polythermal (i.e., locally wet-based), given that these deposits suggest high sediment supply and abundant meltwater at the glacier base, thus great capability for substrate erosion. In addition, common presence of facetted (and rarely striated) clasts (Fig. 5a) argue for wet-based conditions and subglacial clast transport. The presence of gravelly-sand lenses within weakly-bedded diamictites (Dw) supports the idea of basal meltwater availability, mobilized by subglacial channelized currents (glaciofluvial sediments) and then incorporated as rafted blocks. The glacier probably floated over the sea forming an ice shelf, which started to deliver glacial debris near the grounding-line, mostly as subaqueous glacigenic debris flows (depositing Dw and D–Cs lithofacies). As the ice shelf expanded, diamict deposits progressively covered finer distal lithofacies, defining a glacial prograding sedimentary system. Ss lithofacies evidence traction deposition from a sandy turbulent flow in high-regime conditions (hyperpicnic flow), similar to the rippled sands described by Pirrie et al. (1997) deposited in a proximal glaciomarine setting. In distal sectors, dropstones within laminated fine sediments (Ms) are evidence of ice-rafted debris discharge by thawing icebergs (Fig. 9a).

Nelson et al. (2009) suggested that the ice sheet responsible for the deposition of these glacial units was anchored somewhere north of MH

and nourished by rocks from James Ross Island, given the low percentage (<1%) of Antarctic Peninsula-derived erratic clasts. They postulated that an elevation (i.e., volcanic landform) must have existed in order to hold an ice cap. According to these authors, this positive relief was located somewhere near present-day Davies Dome or Prince Gustav Channel, and was later completely removed by erosion. Our observations indicate that the percentage of Antarctic Peninsula-derived clasts is not as low (~5 %) as the one postulated (<1 %) by Nelson et al. (2009), especially in the weakly-bedded diamictites (Dw), which are lateral equivalents to the D–Cs lithofacies. This presumed volcanic massif must have been formed around ~6.2 Ma, which is the minimum age for deposition of the glacial lithofacies. North of the study area, the oldest available ages on in-situ rocks are ~5.6 Ma in Davies Dome (Kristjánsson et al., 2005) and ~5.8 Ma in Cape Lachman (Nývlt et al., 2011), which are too young for the rocks to be remnants of the volcanic massif postulated by Nelson et al. (2009). We argue instead that the ice sheet responsible for the deposition of glacial lithofacies associated with U1 unconformity was anchored on the Antarctic Peninsula and not on a local volcanic massif located at James Ross Island's northern tip, in agreement with a late Miocene glacier advance postulated by Nývlt et al. (2011). The glacial strata becomes thicker towards the south, therefore we infer a basin deepening in that direction. The deposition probably occurred at a minimum water depth of ~150 m, as inferred from the total thickness of the glacial strata (Nelson et al., 2009), thus corresponding to a shallow marine shelf.

6.1.2. Eruptive Stage 1

After the ice sheet advance, volcanic activity resumed with the deposition of Unit 1 lithofacies, mainly associated with emplacement of a prograding lava-fed delta system towards the south-southeast (Fig. 9b). This system has lateral associations with finer pyroclastic lithofacies in more distal portions, such as planar- and cross-stratified tuffs (Tsc) and laminated tuffaceous mudstones (Ms). Especially at MH, pillow breccia (Bpw) clinoforms present a complex architecture and are commonly separated by erosive unconformities (Fig. 9b), which speak either for eustatic sea level changes during volcanic activity (e.g., Jones and Nelson, 1970) or, more likely, differential subsidence of the delta front (Kauahikaua et al., 1993), allowing an increment in the accommodation space and retrogradation of the volcaniclastic system (relative sea level changes). Lava-fed hyaloclastite deltas are almost always prograding depositional systems, and compared to clastic delta systems, they are characterized by high-supply of volcanic material, which efficiently fills the available accommodation space and generates rapid basinward shifting of the shoreline, on short geological timescales (e.g., Wright et al., 2012). The different sets of foreset-bedded breccias suggest discrete pulses of volcanism and each delta unit thickness reflects the available accommodation space at the time of eruptions (i.e., approximate water level). During delta build out, both lava benches and the delta front may have suffered collapses as high-density subaqueous debris flows (e.g., Sansone and Smith, 2006) (Fig. 9c). Collapse trigger could have been related to subsidence of the lava bench due to lava tube activity (Mattox and Mangan, 1997), wave action or processes related to lateral shifting of the subaerial lava streams, all of which could have also affected the height of the resulting passage zones (e.g., Watton et al., 2013). On the other hand, delta edge collapse may have also triggered littoral explosions (Mattox and Mangan, 1997), which even though no clear deposits of such explosions have been found, were likely to occur.

The radiometric age for this lava-fed delta was bracketed between ca. 6.2 and 5.9 Ma by Kristjánsson et al. (2005). Our new unspiked K–Ar age data demonstrates that subaerial lavas emitted from vent/s at CSM (Fig. 9c), are considerably younger (5.2–4.6 Ma) than the ages reported by Kristjánsson et al. (2005). Lava-fed delta systems are formed within very short periods of time (Wright et al., 2012; Watton et al., 2013), which is why this ~1 Myr difference suggests that at least two different lava-fed delta systems, an older one fed by an unrecognized vent/s north of CSM (between 6.2 and 5.9 Ma) and a younger one fed by CSM volcano (between 5.2 and 4.6 Ma), formed Unit 1 lava-fed delta lithofacies in the study area, but each one formed very rapidly. An erosive (probably glacial in origin) unconformity must be present between the two lava-fed delta systems, but such an unconformity is still unrecognized. Vents centered at CMS during Stage 1 were mainly subaerial, as evidenced by cinder cone deposits and a large volcanic conduit/lava lake which fed a volcanic apparatus on the surface, now removed by erosion (Fig. 9c). These vents emitted pāhoehoe-type, compound lava flows which allowed building and progradation of the lava-fed delta system towards the south (Fig. 9c).

The nature of the water body where the lava-fed delta system was deposited is a matter of debate. Three possibilities emerge, namely (1) the sea, (2) an englacial lake formed as a subglacial melting product of direct lava-ice contact or (3) a non-glacial lake. Several authors attempted to distinguish between marine or non-marine (englacial and non-glacial lacustrine) lava-fed deltas (e.g., Werner and Schmincke, 1999; Skilling, 2002; Smellie, 2006). One of the most widely used criteria for distinguishing between the two options is the variation in passage zone levels (Smellie, 2006). Smellie (2006) argued that in marine lava-fed delta sequences, passage zones present relatively constant altitudes (subhorizontal) along several kilometers. In contrast, during the emplacement of englacial lava-fed deltas, the water level in the ice-enclosed lake is usually a very dynamic feature as a result of several drainage systems both sub and supraglacially. In consequence, rapid drops in the lake water level during the course of an eruption will cause passage zone altitude variations along short horizontal distances. For the lava-fed delta system of Unit 1, the passage zone altitude is relatively constant and subhorizontal, with an overall falling angle of ~2° over a long distance (>7 km), which implies a stable water level during the course of the eruption/s (Smellie, 2006). As mentioned, tabular lava flows usually show features of subaqueous flow, such as pillowed margins or intercalation with massive hyaloclastite beds. Thus, lava-breccia clinoform contacts (i.e., passage zone) do not always represent the water level at the time of delta formation. Moreover, as pointed out by Watton et al. (2013), factors such as lava flux rate, the accommodation space and coastline morphology may all affect the resulting height of the passage zone.

On the other hand, the close relationship with fossil-bearing glaciomarine deposits (U1 unconformity) strongly suggests that lava-fed delta deposition occurred in a shallow (~200 m) marine environment (Fig. 9b–c). It should be noted that multi-proxy paleoclimatic data obtained in the Antarctic Peninsula region suggest that several ice-poor, interglacial periods took place during late Miocene and early Pliocene times (e.g., Joseph et al., 2002; McArthur et al., 2006; Smellie et al., 2006a; Nelson et al., 2009; Nývlt et al., 2011; Pirrie et al., 2011) but given the short-term glacial/interglacial cyclicity (see Nývlt et al., 2011), it may be difficult to ensure, with the available age data, that both pulses of activity (6.2–5.9 and 5.2–4.6 Ma) of lava-fed delta formation during Eruptive Stage 1 occurred during ice-poor, interglacial periods, where marine eruptive conditions could have prevailed.

6.1.3. Unconformity U2

Unit 1 lithofacies were truncated by the development of U2 unconformity, which is represented at CSM by massive diamictites interpreted as lodgement tills, overlying glacially-striated pāhoehoe-type lava flows. This striated pavement shows SW–NE striae orientation, suggesting this paleo-ice flow orientation. The predominance of locally-derived basaltic clasts in this diamictite speaks for a James Ross Island-nourished ice cap, which may have flowed from the southwest. At MH, U2 unconformity gradually descends to the south, from ~500 to ~350 m a.s.l. No glacial deposits were found in the northern sections of MH, but pāhoehoe-type lava flows of Unit 1 have glacially-eroded tops, with E–W and SW–NE striae orientation. The presence of this unconformity within the eruptive sequence suggests a period of volcanic quiescence followed by glacial advance and erosion.

The glacier responsible for erosion and till deposition was locally wet-based (polythermal), given that lodgement tills resting on ice-modified surfaces (striated pavements) indicate basal water availability and strong subglacial erosion. Volcanic activity during this time must have been dormant, allowing glacial erosion of older (Unit 1) deposits, as also suggested by Hambrey and Smellie (2006) to explain the deposition of diamictite levels within the volcanic succession. In CSM, the youngest pre-U2 units are pāhoehoe-type lava flows with striated tops, with an age of 4.63 ± 0.28 Ma (early Pliocene). We propose this maximum age for the glacial advance responsible for U2 unconformity carving. Massive pillow lavas with an early Pliocene age of 4.31 ± 0.26 Ma overlie U2 glacial deposits, considered here as the minimum age for the glacial advance. Considering errors, this glacigenic unit deposition (i.e., glacial advance) occurred somewhere between 4.9 and 4.0 Ma. However, timing for this diamictite deposition most probably resembles the age of the overlying eruptive unit (Unit 2), namely the interval 4.6–4.0 Ma. This agrees with previous postulates which suggest that after ca. 4.6 Ma, a James Ross Island-centered ice cap overrode previous eruptive units, depositing glacial strata with almost complete predominance of JRIVG-derived volcanic clasts (Hambrey et al., 2008; Smellie et al., 2008). On the other hand, two different intravolcanic glacial levels are exposed at the southern end of MH (Fig. 6c). The lower level bears abundant marine shell fragments and large proportion of erratic clasts speaking for an Antarctic Peninsula-anchored glacier, and separated from the upper glacial level by a ~10 m thick pillow breccia deposit. This arrangement raises the possibility that almost contemporaneously with expansion of local ice caps (James Ross Island-centered), glaciers from the Antarctic Peninsula may have expanded as well (see Smellie et al., 2009 and references therein), depositing glacial diamictites within the volcanic sequence. The presence of marine shell fragments included in the diamictites is controversial, given that they may be good proxies for glaciomarine deposition (Nelson et al., 2009) or could be reworked from older glaciomarine deposits (Smellie et al., 2006a; Nývlt et al., 2011).

6.1.4. Eruptive Stage 2

Between 120 and 200 m of volcanic pile (Unit 2) overlies U2-related glacial deposits and associated erosive surfaces. At CSM, massive pillow lavas and pillow breccias overlie glacigenic diamictites at a constant altitude of 620 m a.s.l. "Squeeze-up" structures reflect nearly coeval deposition of U2 glacial deposits and overlying subaqueous volcanics (pillow lavas). Moreover, the base of Unit 2 is located at >600 m a.s.l in the present-day. If Unit 2 deposition occurred in a marine environment, a 600 m uplift of the volcanic pile must have taken place. Such uplift might take place tectonically, but there is no record of such a tectonic scenario in James Ross Island during Neogene times. Another possibility is uplift from postglacial rebound. Marine eruptive conditions would imply postglacial rebounds of >600 m that require former ice sheets >2.5 km thick, which is highly unlikely for this region due to its relatively low latitude. On the other hand, another lava-fed delta system was created at the last phases of Stage 2, with a passage zone which is well-defined only at CSM and MH's northern portion, but completely absent at MH's central and southern portions. However, we were able to detect that, in MH northern section, passage zone is found higher as we head south (i.e., in the direction of delta progradation), with a gentle mean rising angle of ~3°. In the scheme of Smellie (2006), this subaqueous/subaerial transition falls in the category of rising passage zones, which are believed to form in non-stable coeval water bodies (i.e., englacial lakes). Overall, we argue that the most likely scenario for Eruptive Stage 2 was related to volcano interaction with glacial ice (i.e., glaciovolcanism; Smellie, 2006).

In this scenario, eruptive activity was centered at CSM polygenetic volcano and began with lavas in direct contact with ice, leading to ice cap melting at its base and formation of an englacial meltwater vault. Here, the hydrostatic pressure was high enough to prevent lava fragmentation, thus leading to basal pillow lava formation as isolated pillow mounds. These pillow mounds usually suffered from mass-flow wasting processes (Fig. 9d), forming massive pillow breccias (Bpm lithofacies). High-density sediment gravity flows (density currents) also distributed pyroclastic material away from the vent and were probably channeled through subglacial drainage systems. Very distal portions of these density currents are represented by laminated tuffaceous mudstones and siltstones (Ms) exposed at MH (Fig. 9d). As the englacial volcano started to grow both vertically and laterally, the glacier roof collapsed, forming an ice-enclosed meltwater lake (Fig. 9e). These lakes are part of very dynamic hydraulic systems, where water is drained by different mechanisms, either supra- or sub-glacially (Smellie, 2006). Meltwater escape combined with vertical growth of the volcanic pile implied a decrease in hydrostatic pressure which triggered explosive hydrovolcanic eruptions (Fig. 9e), related to a shallow (maybe less than 100 m) emergent volcano, as suggested elsewhere (see Smellie and Hole, 1997). These eruptions are represented by massive tuff breccias and bedded lapilli tuffs (TB–LTs lithofacies) in CSM, whereas in MH they correspond to T–LTw distal lithofacies. Lack of accidental clasts and high flow regime sedimentary structures (dunes, antidunes) suggest a clear vent continuously flooded with water, typical of wet, Surtseyan-type eruptions during volcano emergence (Sheridan and Wohletz, 1983; Kokelaar, 1986; Sohn and Chough, 1992; White, 1996). TB–LTs lithofacies represent near-vent deposits of debris flows that were products of rapid tephra pile-up and high slopes. Poor bedding in the T-LTw lithofacies indicates a high tephra input, probably related to continuous uprush during the formation of a subaqueous eruptive column (e.g., Smellie, 2000). Normal-graded beds may indicate that highly concentrated tephra flows were probably deposited as subaqueous fallout or even by vertical density currents (Manville and Wilson, 2004) from a tephra plume. Better development of lamination and bed thinning in the tuff beds (Fig. 7e) suggest a lower magma output and waning explosive activity (Smellie, 2000). Similar deposits were described in the tuff cone deposits exposed at Bibby Hill (Fig. 1, Nehyba and Nývlt, 2014). The presence of a facetted and striated basaltic lithoclast incorporated in the T–LTw lithofacies (Fig. 7e) indicates that either it was expelled as a lithoclast during the course of the hydromagmatic eruption or it was transported by thawing icebergs, and then released and incorporated in the tephra unit. Smellie et al. (2008) inferred that the source of the "yellow band" at MH (T–LTw lithofacies) was related to a marine tuff cone located somewhere near Seacatch Nunataks (see Fig. 1), 5 km west of MH, while we believe that CSM was the source during this glaciovolcanic stage. This is supported by the fact that the available ages from Seacatch Nunataks of ~5.9 Ma (Smellie et al., 2008) contrast with our 4.6–4.0 Ma ages for Unit 2.

At CSM, volcanic activity continued with the intrusion and subsequent extrusion of subaqueous, columnar-jointed basalt (Fj lithofacies), which suffered sudden cooling due to direct contact with external water. The package of subaerial lava flows that overlies Fj lithofacies suggests that the glaciovolcanic pile finally emerged, completing the ideal evolution of a Tuya-type volcanic edifice (Mathews, 1947), which are flat-topped volcanoes formed by subaqueous to emergent volcanic sequences and capped by subaerial lava-fed deltas. As mentioned earlier, these lava flows overlie the prograding sets of foreset-bedded pillow breccias at MH's northern section, defining a gentle rising passage zone (Fig. 9f), which according to Smellie (2006), may be diagnostic of an englacial setting. A rising passage zone indicates that the rate of the lake water level rise is higher than the rate of aggradation at the delta front, i.e., the delta surface was locally flooded. The rising water level may be associated with water displacement due to delta advance, favored by temporarily blockages in the drainage system due to delta front collapses (Smellie, 2006).

The total thickness of ~200 m of the subaqueous eruptive units is a good proxy of the englacial lake depth at the moment of eruptions. To have an approximate constraint on the ice sheet thickness, we need first to consider a permeable upper layer in the glacier, composed of snow/firn and fractured ice, which behaves as an upper limit of the

englacial lake water level (Smellie, 2000; Smellie et al., 2008). Smellie et al. (2011) considered that a good estimate of the thickness of this upper permeable snow/firn and fractured ice layer is around 100 m. Therefore, for our study area, we infer an ice sheet thickness ~300 m, which is within the range of Smellie et al.'s (2008) ice thickness estimates of 200–750 m for the Neogene in the James Ross Island area. It should be noted, however, that glaciovolcanic sequences may be formed even during ice-poor, interglacial periods, such as the present-day, especially in high latitude regions (Smellie et al., 2008). Even within James Ross Island, the higher lying areas remain glaciated, while in coastal areas ice-free, interglacial conditions prevail. Thus, we agree with previous postulates (e.g., Johnson et al., 2009; Smellie et al., 2009) that in the majority of these so-called "interglacial" periods, ice-poor rather than ice-free conditions prevailed.

Regarding the age of the eruptive units assigned to Eruptive Stage 2, the available data is somewhat contradictory. The unit of columnar-jointed basalts (lithofacies Fj) was dated by Kristjánsson et al. (2005) and gave a $^{40}Ar/^{39}Ar$ age of 5.14 ± 0.38 Ma, which is in conflict with our unspiked K–Ar age of ~4.3 Ma for stratigraphically older pillow lavas. However, considering errors, it is plausible that both units originated around 4.7–4.5 Ma. On the other hand, age data from Sykes (1988) and Kristjánsson et al. (2005) for MH, combined with our unrealistic ~4.4 Ma age data, suggest that Eruptive Stage 2 occurred around 4.6–4.0 Ma (early Pliocene). Unfortunately, until more detailed geochronological data become available, we tentatively conclude that Unit 2 volcanics were emplaced sometime after 4.6 Ma.

6.2. Correlation with Lachman Crags

It is worth mentioning that this work focused on the eruptive products of CSM vent/s and their progradation towards the south, forming MH eruptive units. However, progradation of volcanic products towards the north was also plausible, and the possibility arises that part of the volcanic pile forming Lachman Crags (Fig. 1) was emitted from CSM volcano. Although we have not yet performed detailed stratigraphic work at Lachman Crags, the results obtained by De Angelis (1999) provide us with an excellent stratigraphic framework of that area. This author distinguished seven eruptive units, the oldest one represented by a large intrusive body at the northern end, which has a K–Ar age of 5.23 ± 0.57 Ma (Sykes, 1988). This intrusion was glacially-truncated and covered by glacial diamictites bearing marine fossils. A lava-fed delta system which prograded towards the north affords ages between ~5.3 and ~4.6 Ma (Sykes, 1988; Smellie et al., 2008), which are surprisingly coincident with our interpretation that eruptive activity centered at CSM took place between 5.2 and 4.6 Ma. Moreover, Smellie et al. (2008) speculated that this lava-fed delta (their Lachman Crags Main Delta) was fed by a satellite center at its southern margin and could have been emplaced in a marine setting, coincident with our interpretation that, during Eruptive Stage 1, deposition of the hyaloclastite lava-fed delta occurred in a shallow marine environment. Bottomset deposits related to this lava-fed delta sequence show different distribution of lithofacies probably caused by local conditions related to the slopes of a subaqueous volcano (Nehyba and Nývlt, 2015), which we infer was CSM. De Angelis (1999) also recognized an intravolcanic glacial unconformity at 540 m a.s.l. (southern end of Lachman Crags) which gradually descends to the north, where it is found at 460 m a.s.l. This unconformity is associated with massive diamictites lacking marine shell fragments of any kind and a clast population suggesting a strong JRIVG-provenance. Overlying this unconformity, poorly foreset-bedded pillow breccias are covered by a thin package of tabular lava flows, probably related to a glaciovolcanic eruptive environment as well (De Angelis, 1999) (Fig. 9f). This arrangement is strongly similar to what is found at CSM and MH associated with U2 unconformity. Age constraints for these units come from an early Pliocene $^{40}Ar/^{39}Ar$ age of 3.95 ± 0.05 Ma (Kristjánsson et al., 2005), which is slightly younger than eruptive units ascribed to Eruptive Stage 2 (4.6–4.0 Ma). Although not conclusive, a strong correlation seems to arise between the volcano-epiclastic stratigraphy at Lachman Crags, CSM and MH, suggesting a common link between them. Clearly much more work is needed to support this connection.

7. Conclusions

Detailed lithofacies analysis of volcanic and glacial deposits of the JRIVG in Cerro Santa Marta area, supported by new unspiked K–Ar ages, allows an improved understanding of eruptive environments and paleoclimate between 6.2 (late Miocene) and 4.3 Ma (early Pliocene). The following main conclusions can be drawn:

(1) A glacial advance carved an erosive unconformity (U1) on the Cretaceous bedrock and older volcanic units, and it was related to deposition of diverse glacial lithofacies related to an Antarctic Peninsula Ice Sheet expansion sometime between ~7.2 and 6.6 Ma (Grützner et al., 2005). The ice sheet was most likely locally wet-based (polythermal regime). It probably floated over the sea (ice shelf) towards the south-southeast and deposited mostly subaqueous glacial lithofacies, in places bearing marine shell fragments.

(2) Shortly after that, the ice sheet must have retreated, and renewed volcanic activity began (Eruptive Stage 1). It was characterized by the extrusion of subaerial, pāhoehoe-type lava flows fed from an unrecognized vent north of the study area between 6.2 and 5.9 Ma (ages according to Kristjánsson et al., 2005). These lava flows probably penetrated the sea forming a laterally extensive (>7 km) lava-fed delta. Later, volcanic vents shifted to Cerro Santa Marta volcano, emitting more lava flows that fed the same hyaloclastite delta sequence towards the south, at Massey Heights. This vent shifting occurred between 5.2 and 4.6 Ma (early Pliocene).

(3) A second glacial advance in the region, probably coinciding with a pause in volcanic activity, eroded older volcanic rocks (Unit 1) and deposited subglacial (lodgement) tills. The ice cap was James Ross Island-centered and flowed mainly to the east and northeast, but probably coalesced with glaciers flowing from the Antarctic Peninsula. Coeval with the glacier presence in the area, volcanic activity restarted at CSM polygenetic volcano. Tuya-forming, glaciovolcanic eruptions formed another lava-fed delta which prograded towards Mt. Haddington. From detailed measures of subaqueous unit thicknesses and passage zone altitudes, we can infer that the glacier was ~300 m thick, in good agreement with previously inferred Neogene paleo-ice thickness in the area. According to published and new radiometric data, we believe that this local glacial advance occurred between 4.6 and 4.0 Ma (early Pliocene).

(4) Although not conclusive, the available geological information allows us to infer that a strong link exists between eruptive units exposed at Lachman Crags and those emitted from Cerro Santa Marta volcano and its counterpart further south at Massey Heights. Future work in the area would help test this suggestion.

Acknowledgments

We want to express our gratitude to the personnel of the Instituto Antártico Argentino (IAA), Dirección Nacional del Antártico (DNA) and Fuerza Aérea Argentina, for their logistic support over the last 25 years. The English version of this article was enormously improved by Bárbara Boltshauser. Our most sincere gratitude to Federico Martina, Santiago Maza, Juan Presta and Mike Kaplan for their help during field work. Prof. Keisuke Nagao, from the University of Tokyo, kindly supported us during unspiked K–Ar age dating. We kindly appreciate very useful suggestions and comments made by Daniel Nývlt and one

anonymous reviewer. We also thank the thorough revisions made by the editor Joan Martí. This work was funded by PICTO 2002 11573, SECyT-CONICET "Morfogénesis del extremo sur de Sudamérica, Arco de Scotia y Península Antártica", granted to J.A.S.

Appendix A. Supplementary data

Supplementary data to this article can be found online at http://dx.doi.org/10.1016/j.jvolgeores.2015.03.011.

References

Aitkenhead, N., 1975. The geology of the Duse Bay-Larsen Inlet area, North-East Graham Land. Brit. Antarct. Surv. Sci. Rep. 51, 62.

Bibby, J.S., 1966. The stratigraphy of part of north-east Graham Land and the James Ross Island Group. Brit. Antarct. Surv. Sci. Rep. 53, 51.

Carrizo, H.G., Torielli, C.A., Strelin, J.A., Muñoz, C.E., 1998. Ambiente eruptivo del Grupo Volcánico Isla James Ross en Riscos Rink, isla James Ross, Antártida. Rev. Asoc. Geol. Argent. 53, 469–479.

Catuneanu, O., 2002. Sequence stratigraphy of clastic systems: concepts, merits, and pitfalls. J. Afr. Earth Sci. 35, 1–43. http://dx.doi.org/10.1016/S0899-5362(02)00004-0.

Czech Geological Survey, 2009. James Ross Island — northern part. Topographic map 1: 25 000. CGS, Praha.

De Angelis, D.H., 1999. Ambiente eruptivo del Grupo Volcánico Isla James Ross en Riscos Lachman, isla James Ross, Antártida. (M.A. Thesis), University of Buenos Aires, Argentina 128 pp.

del Valle, R.A., Elliot, D.H., Macdonald, D.I.M., 1992. Sedimentary basins on the east flank of the Antarctic Peninsula: proposed nomenclature. Antarct. Sci. 4, 477–478.

Edwards, B.R., Russell, J.K., Anderson, R.G., 2002. Subglacial, phonolitic volcanism at Hoodoo Mountain volcano, northern Canadian Cordillera. Bull. Volcanol. 64, 254–272. http://dx.doi.org/10.1007/s00445-002-0202-9.

Elsworth, D., Voight, B., 1995. Dike intrusion as a trigger for large earthquakes and the failure of volcano flanks. J. Geophys. Res. 100, 6005–6024. http://dx.doi.org/10.1029/94JB02884.

Engel, Z., Nývlt, D., Láska, K., 2012. Ice thickness, areal and volumetric changes of Davies Dome and Whisky Glacier (James Ross Island, Antarctic Peninsula) in 1979–2006. J. Glaciol. 58, 904–914. http://dx.doi.org/10.3189/2012JoG11J156.

Grützner, J., Hillenbrand, C.D., Rebesco, M., 2005. Terrigenous flux and biogenic silica deposition at the Antarctic continental rise during the late Miocene to early Pliocene: implications for ice sheet stability and sea ice coverage. Glob. Planet. Chang. 45, 131–149. http://dx.doi.org/10.1016/j.gloplacha.2004.09.004.

Hambrey, M.J., McKelvey, B., 2000. Neogene fjordal sedimentation on the western margin of the Lambert Graben, East Antarctica. Sedimentology 47, 577–607. http://dx.doi.org/10.1046/j.1365-3091.2000.00308.x.

Hambrey, M.J., Glasser, N.F., 2003. Glacial sediments: processes, environments and facies. In: Middleton, G.V. (Ed.), Encyclopedia of Sediments and Sedimentary Rocks. Springer, Dordrecht, pp. 316–331.

Hambrey, M.J., Smellie, J.L., 2006. Distribution, lithofacies and environmental context of Neogene glacial sequences on James Ross and Vega islands, Antarctic Peninsula. In: Francis, J.E., Pirrie, D., Crame, J.A. (Eds.), Cretaceous–Tertiary High-Latitude Paleoenvironments, James Ross Basin, Antarctica. Geological Society, London, Special Publications 258, pp. 187–200.

Hambrey, M.J., Smellie, J.L., Nelson, A.E., Johnson, J.S., 2008. Late Cenozoic glacier–volcano interaction on James Ross Island and adjacent areas, Antarctic Peninsula region. Geol. Soc. Am. Bull. 120, 709–731. http://dx.doi.org/10.1130/B26242.1.

Hole, M.J., Saunders, A.D., Rogers, G., Sykes, M.A., 1995. The relationship between alkaline magmatism, lithospheric extension and slab window formation along continental destructive plate margins. In: Smellie, J.L. (Ed.), Geological Society, London, Special Publications 81, pp. 265–285.

Johnson, J.S., Smellie, J.L., Nelson, A.E., Stuart, F.M., 2009. History of the Antarctic Peninsula Ice Sheet since the early Pliocene — evidence from cosmogenic dating of Pliocene lavas on James Ross Island, Antarctica. Glob. Planet. Chang. 69, 205–213. http://dx.doi.org/10.1016/j.gloplacha.2009.09.001.

Jones, J.R., Nelson, P.H.H., 1970. The flow of basalt lava from air into water: its structural expression and stratigraphic significance. Geol. Mag. 107, 13–21.

Jonkers, H.A., 1998. The Cockburn Island Formation; Late Pliocene interglacial sedimentation in the James Ross Basin, northern Antarctic Peninsula. Newsl. Stratigr. 36, 63–76.

Jonkers, H.A., Lirio, J.M., del Valle, R.A., Kelley, S.P., 2002. Age and environment of Miocene–Pliocene glaciomarine deposits, James Ross Island, Antarctica. Geol. Mag. 139, 577–594. http://dx.doi.org/10.1017/S0016756802006787.

Joseph, L.H., Rea, D.K., van der Pluijm, B.A., Gleason, J.D., 2002. Antarctic environmental variability since the late Miocene: ODP Site 745, the East Kerguelen sediment drift. Earth Planet. Sci. Lett. 201, 127–142. http://dx.doi.org/10.1016/S0012-821X(02)00661-1.

Kauahikaua, J., Denlinger, R., Foster, J., Keszthelyi, L., 1993. Lava delta instability: is it mass wasting or is it triggered by lava flowing through tubes? Eos 74, 616.

Kokelaar, P., 1986. Magma–water interactions in subaqueous and emergent basaltic volcanism. Bull. Volcanol. 48, 275–289. http://dx.doi.org/10.1007/BF01081756.

Košler, J., Magna, T., Mlčoch, B., Mixa, P., Nývlt, D., Holub, F.V., 2009. Combined Sr, Nd, Pb and Li isotope geochemistry of alkaline lavas from northern James Ross Island (Antarctic Peninsula) and implications for back-arc magma formation. Chem. Geol. 258, 207–218. http://dx.doi.org/10.1016/j.chemgeo.2008.10.006.

Kristjánsson, L., Gudmundsson, M.T., Smellie, J.L., McIntosh, W.C., Esser, R., 2005. Palaeomagnetic, $^{40}Ar/^{39}Ar$, and stratigraphical correlation of Miocene–Pliocene basalts in the Brandy Bay area, James Ross Island, Antarctica. Antarct. Sci. 17, 409–417. http://dx.doi.org/10.1017/S0954102005002853.

Lawver, L.A., Keller, R.A., Fisk, M.R., Strelin, J., 1995. Bransfield Strait, Antarctic Peninsula: active extension behind a dead arc. In: Taylor, B. (Ed.), Backarc Basins: Tectonics and Magmatism. Plenum Press, Holland, pp. 315–342.

Lirio, J.M., Núñez, H.J., Bertels-Psotka, A., del Valle, R.A., 2003. Diamictos fosilíferos (Mioceno–Pleistoceno): Formaciones Belén, Gage y Terrapin en la isla James Ross, Antártida. Rev. Asoc. Geol. Argent. 58, 298–310.

Lønne, I., 1995. Sedimentary facies and depositional architecture of ice-contact glaciomarine systems. Sediment. Geol. 98, 13–43.

Lowe, D.R., 1982. Sediment gravity flows: II. Depositional models with special reference to the deposits of high-density turbidity currents. J. Sediment. Petrol. 52, 279–297. http://dx.doi.org/10.1306/212F7F31-2B24-11D7-8648000102C1865D.

Maicher, D., White, J.D.L., Batiza, R., 2000. Sheet hyaloclastite: density-current deposits of quench and bubble burst fragments from thin, glassy sheet lava flows, Seamount Six, Eastern Pacific Ocean. Mar. Geol. 171, 75–94. http://dx.doi.org/10.1016/S0025-3227(00)00109-2.

Manville, V., Wilson, C.J.N., 2004. Vertical density currents: a review of their potential role in the deposition and interpretation of deep-sea ash layers. J. Geol. Soc. Lond. 161, 947–958. http://dx.doi.org/10.1144/0016-764903-067.

Marenssi, S.A., Casadío, S., Santillana, S.N., 2010. Record of Late Miocene glacial deposits on Isla Marambio (Seymour Island), Antarctic Peninsula. Antarct. Sci. 22, 193–198. http://dx.doi.org/10.1017/S0954102009990629.

Massabie, A.C., Morelli, J.R., 1977. Buchitas de la isla Vicecomodoro Marambio, Sector Antártico Argentino. Rev. Asoc. Geol. Argent. 32, 44–51.

Mathews, W.H., 1947. "Tuyas", flat-topped volcanoes in northern British Columbia. Am. J. Sci. 245, 560–570.

Mattox, T.N., Mangan, M.T., 1997. Littoral hydrovolcanic explosions: a case study of lava–seawater interaction at Kilauea Volcano. J. Volcanol. Geotherm. Res. 75, 1–17. http://dx.doi.org/10.1016/S0377-0273(96)00048-0.

McArthur, J.M., Rio, D., Massari, F., Castradori, D., Bailey, T.R., Thirlwall, M., Houghton, S., 2006. A revised Pliocene record for marine $^{87}Sr/^{86}Sr$ used to date an interglacial event recorded in the Cockburn Island Formation, Antarctic Peninsula. Palaeogeogr. Palaeoclimatol. Palaeoecol. 242, 126–136. http://dx.doi.org/10.1016/j.palaeo.2006.06.004.

Nehyba, S., Nývlt, D., 2014. Deposits of pyroclastic mass flows at Bibby Hill (Pliocene, James Ross Island, Antarctica). Czech Polar Rep. 4, 103–122.

Nehyba, S., Nývlt, D., 2015. "Bottomsets" of the lava-fed delta of James Ross Island Volcanic Group, Ulu Peninsula, James Ross Island, Antarctica. Polish Polar Research 36, 1–24. http://dx.doi.org/10.1515/popore-2015-0002.

Nelson, P.H.H., 1975. The James Ross Island Volcanic Group of north-east Graham Land. Brit. Antarct. Surv. Sci. Rep. 54, 1–89.

Nelson, A.E., Smellie, J.L., Hambrey, M.J., Williams, M., Vautravers, M., Salzmann, U., McArthur, J.M., Regelous, M., 2009. Neogene glacigenic debris flows on James Ross Island, northern Antarctic Peninsula, and their implications for regional climate history. Quat. Sci. Rev. 28, 3138–3160. http://dx.doi.org/10.1016/j.quascirev.2009.08.016.

Németh, K., Martin, U., 2007. Shallow sill and dike complex in western Hungary as a possible feeding system of phreatomagmatic volcanoes in "soft-rock" environment. J. Volcanol. Geotherm. Res. 159, 138–152. http://dx.doi.org/10.1016/j.jvolgeores.2006.06.014.

Németh, K., Cronin, S.J., 2008. Volcanic craters, pit craters and high-level magma-feeding systems of a mafic island-arc volcano: Ambrym, Vanuatu, South Pacific. In: Thomson, K., Petford, N. (Eds.), Structure and Emplacement of High-Level Magmatic Systems. Geological Society, London, Special Publications 302, pp. 87–102.

Nývlt, D., Košler, J., Mlčoch, B., Bubík, M., Hendriks, B.W.H., 2011. The Mendel formation: implication for Late Miocene climatic cyclicity at the northern tip of the Antarctic Peninsula. Palaeogeogr. Palaeoclimatol. Palaeoecol. 299, 363–384. http://dx.doi.org/10.1016/j.palaeo.2010.11.017.

Pirrie, D., Crame, J.A., Riding, J.B., Butcher, A.R., Taylor, P.D., 1997. Miocene glaciomarine sedimentation in the Northern Antarctic Peninsula region: the stratigraphy and sedimentology of the Hobbs Glacier Formation, James Ross Island. Geol. Mag. 136, 745–762. http://dx.doi.org/10.1017/S0016756897007796.

Pirrie, D., Jonkers, H.A., Smellie, J.L., Crame, J.A., McArthur, J.M., 2011. Reworked late Neogene *Austrochlamys anderssoni* (Mollusca: Bivalvia) from northern James Ross Island, Antarctica. Antarct. Sci. 23, 180–187. http://dx.doi.org/10.1017/S0954102010000842.

Porębski, S.J., Gradzinski, R., 1990. Lava-fed Gilbert-type delta in the Polonez Cove Formation (Lower Oligocene), King George Island, West Antarctica. In: Colella, A., Prior, D.B. (Eds.), Coarse-grained Deltas. Blackwell Scientific Publications, International Association of Sedimentologists, Oxford, Special Publication 10, pp. 335–354.

Rex, D.C., 1976. Geochronology in relation to the stratigraphy of the Antarctic Peninsula. Brit. Antarct. Surv. Bull. 43, 49–58.

Sansone, F.J., Smith, J.R., 2006. Rapid mass wasting following nearshore submarine volcanism on Kilauea volcano, Hawaii. J. Volcanol. Geotherm. Res. 151, 133–139. http://dx.doi.org/10.1016/j.jvolgeores.2005.07.026.

Self, S., Keszthelyi, L., Thordarson, T., 1998. The importance of Pāhoehoe. Annu. Rev. Earth Planet. Sci. 26, 81–110. http://dx.doi.org/10.1146/annurev.earth.26.1.81.

Sheridan, M.F., Wohletz, K.H., 1983. Hydrovolcanism: basic considerations and review. J. Volcanol. Geotherm. Res. 17, 1–29. http://dx.doi.org/10.1016/0377-0273(83)90060-4.

Skilling, I.P., 1994. Evolution of an englacial volcano: Brown Bluff, Antarctica. Bull. Volcanol. 56, 573–591. http://dx.doi.org/10.1007/BF00302837.

Skilling, I.P., 2002. Basaltic pahoehoe lava-fed deltas: large-scale characteristics, clast generation, emplacement processes and environmental discrimination. In: Smellie, J.L., Chapman, M.G. (Eds.), Volcano–Ice Interaction on Earth and Mars. Geological Society, London, Special Publication 202, pp. 91–113.

Smellie, J.L., 1990. D. Graham Land and South Shetland Islands. In: LeMasurier, W.E., Thomson, J.W. (Eds.), Volcanoes of the Antarctic Plate and Southern Oceans. Antarctic Research Series No. 48. American Geophysical Union, Washington DC, pp. 303–359.
Smellie, J.L., 1999. Lithostratigraphy of Miocene-Recent, alkaline volcanic fields in the Antarctic Peninsula and eastern Ellsworth Land. Antarct. Sci. 11, 362–378.
Smellie, J.L., 2000. Subglacial eruptions. In: Sigurdsson, H., Houghton, B., McNutt, S., Rymer, H., Stix, J. (Eds.), Encyclopedia of Volcanoes. Academic Press, San Diego, CA, pp. 403–418.
Smellie, J.L., 2006. The relative importance of supraglacial versus subglacial meltwater escape in basaltic subglacial tuya eruptions: an important unresolved conundrum. Earth Sci. Rev. 74, 241–268. http://dx.doi.org/10.1016/j.earscirev.2005.09.004.
Smellie, J.L., Hole, M.J., 1997. Products and processes in Pliocene-Recent. Subaqueous to emergent volcanism in the Antarctic Peninsula: examples of englacial Surtseyan volcano construction. Bull. Volcanol. 58, 628–646. http://dx.doi.org/10.1007/s004450050167.
Smellie, J.L., Pankhurst, R.J., Hole, M.J., Thomson, J.W., 1988. Age, distribution and eruptive conditions of Late Cenozoic alkaline volcanism in the Antarctic Peninsula and Eastern Ellsworth Land: Review. Brit. Antarct. Surv. Bull. 80, 21–49.
Smellie, J.L., McArthur, J.M., McIntosh, W.C., Esser, R., 2006a. Late Neogene interglacial events in the James Ross Island region, northern Antarctic Peninsula, dated by Ar/Ar and Sr-isotope stratigraphy. Palaeogeogr. Palaeoclimatol. Palaeoecol. 242, 169–187. http://dx.doi.org/10.1016/j.palaeo.2006.06.003.
Smellie, J.L., McIntosh, W.C., Esser, R., Fretwell, P., 2006b. The Cape Purvis Volcano, Dundee Island (northern Antarctic Peninsula): late Pleistocene age, eruptive processes and implications for a glacial palaeoenvironment. Antarct. Sci. 18, 399–408. http://dx.doi.org/10.1017/S0954102006000447.
Smellie, J.L., Johnson, J.S., McIntosh, W.C., Esser, R., Gudmundsson, M.G., Hambrey, M.J., van Wyk De Bries, B., 2008. Six million years of glacial history recorded in the James Ross Island Volcanic Group, Antarctic Peninsula. Palaeogeogr. Palaeoclimatol. Palaeoecol. 260, 122–148. http://dx.doi.org/10.1016/j.palaeo.2007.08.011.
Smellie, J.L., Haywood, A.M., Hillenbrand, C.D., Lunt, D.J., Valdes, P.J., 2009. Nature of the Antarctic Peninsula Ice Sheet during the Pliocene: geological evidence and modeling results compared. Earth Sci. Rev. 94, 79–94. http://dx.doi.org/10.1016/j.earscirev.2009.03.005.
Smellie, J.L., Rocchi, S., Armienti, P., 2011. Late Miocene volcanic sequences in northern Victoria Land, Antarctica: products of glaciovolcanic eruptions under different thermal regimes. Bull. Volcanol. 73, 1–25. http://dx.doi.org/10.1007/s00445-010-0399-y.
Sohn, Y.K., Chough, S.K., 1992. The Ilchulbong tuff cone, Cheju Island, South Korea: depositional processes and evolution of an emergent, Surtseyan-type tuff cone. Sedimentology 39, 523–544.
Strelin, J.A., Malagnino, E.C., 1992. Geomorfología de la isla James Ross. In: Rinaldi, C.A. (Ed.), Geología de la isla James Ross. Instituto Antártico Argentino, Buenos Aires, Argentina, pp. 7–36.
Strelin, J.A., Martino, E., Malagnino, E., 1987. El Cenozoico de la isla James Ross. I Reunión de Comunicaciones sobre Investigaciones Antárticas. Dirección Nacional del Antártico, Buenos Aires, Argentina, p. 72.
Strelin, J.A., Carrizo, H., López, A., Torielli, C., 1993. Actividad volcánica holocena en la isla James Ross. II Jornadas de Comunicaciones sobre Investigaciones Antárticas. Dirección Nacional del Antártico, Buenos Aires, Argentina, pp. 335–340.
Strelin, J.A., Muñoz, C.E., Torielli, C.A., Carrizo, H.G., Medina, F.A., 1997. Las diamictitas de la isla James Ross, Antártida: Origen y probable relación con el "Conglomerado con Pecten". IV Jornadas sobre Investigaciones Antárticas. Dirección Nacional del Antártico, Buenos Aires, Argentina, pp. 328–335.
Sumner, J.M., 1998. Formation of clastogenic lava flows during fissure eruption and scoria cone collapse: the 1986 eruption of Izu-Oshima Volcano, eastern Japan. Bull. Volcanol. 60, 195–212.
Sykes, M.A., 1988. New K–Ar determinations on the James Ross Island Volcanic Group, north-east Graham Land, Antarctica. Brit. Antarct. Surv. Bull. 80, 51–56.
Umino, S., Lipman, P., Obata, S., 2000. Subaqueous lava flow lobes, observed on ROV KAIKO dives off Hawaii. Geology 28, 503–506. http://dx.doi.org/10.1130/0091-7613(2000)28<503:SLFLOO>2.0.CO;2.
Watton, T.J., Jerram, D.A., Thordarson, T., Davies, R.J., 2013. Three-dimensional lithofacies variations in hyaloclastite deposits. J. Volcanol. Geotherm. Res. 250, 19–33. http://dx.doi.org/10.1016/j.jvolgeores.2012.10.011.
Werner, R., Schmincke, H.U., 1999. Englacial vs lacustrine origin of volcanic table mountains: evidence from Iceland. Bull. Volcanol. 60, 335–354. http://dx.doi.org/10.1007/s004450050237.
White, J.D.L., 1996. Pre-emergent construction of a lacustrine basaltic volcano, Pahvant Butte, Utah (USA). Bull. Volcanol. 58, 249–262. http://dx.doi.org/10.1007/s004450050138.
White, J.D.L., 2000. Subaqueous eruption-fed density currents and their deposits. Precambrian Res. 101, 87–109. http://dx.doi.org/10.1016/S0301-9268(99)00096-0.
Williams, M., Smellie, J.L., Johnson, J.S., Blake, D.B., 2006. Late Miocene Asterozoans (Echinodermata) in the James Ross Island Volcanic Group. Antarct. Sci. 18, 117–122. http://dx.doi.org/10.1017/S0954102006000113.
Williams, M., Nelson, A.E., Smellie, J.L., Leng, M.J., Johnson, A.L.A., Jarram, D.R., Haywood, A.M., Peck, V.L., Zalasiewicz, J., Bennett, C., Schöne, B.R., 2010. Sea ice extent and seasonality for the Early Pliocene northern Weddell Sea. Palaeogeogr. Palaeoclimatol. Palaeoecol. 292, 306–318. http://dx.doi.org/10.1016/j.palaeo.2010.04.003.
Wohletz, K.H., 1983. Mechanisms of hydrovolcanic pyroclast formation: grain-size, scanning electron microscopy, and experimental studies. J. Volcanol. Geoth. Res. 17, 31–63. http://dx.doi.org/10.1016/0377-0273(83)90061-6.
Wright, K.A., Davies, R.J., Jerram, D.A., Morris, J., Fletcher, R., 2012. Application of seismic and sequence stratigraphy concepts to a lava-fed delta system in the Faroe-Shetland Basin, UK and Faroes. Basin Res. 24, 91–106. http://dx.doi.org/10.1111/j.1365-2117.2011.00513.x.